



19

Cardiovascular Magnetic Resonance Imaging

RAYMOND Y. KWONG

PRINCIPLES OF MAGNETIC RESONANCE IMAGING, 314

Basic Physics of Magnetic Resonance Imaging, 314

CLINICAL APPLICATIONS OF CMR, 320

Coronary Artery Disease, 320
Cardiomyopathies, 322
Idiopathic Dilated Cardiomyopathy, 326
Other Cardiomyopathies, 327

Valvular Heart Disease, 328
Pericardial Disease, 329

NOVEL CMR IMAGING TECHNIQUES AND FUTURE PERSPECTIVES, 333

REFERENCES, 333

The multicomponent capability of cardiovascular magnetic resonance (CMR) provides morphologic, structural, and physiologic information relevant to a broad array of cardiovascular diseases. CMR offers technical advantages of unrestricted tomographic imaging in arbitrary scan planes, various types of tissue characterization, and a lack of need for ionizing radiation. In this chapter, we will review the current cardiac clinical applications of CMR.

PRINCIPLES OF MAGNETIC RESONANCE IMAGING

Basic Physics of Magnetic Resonance Imaging

Clinical magnetic resonance imaging (MRI) is based on generating signal from the abundant hydrogen nuclei in the human body. When placed inside the magnetic field (called B_0), the ^1H nuclei in a patient's body align with B_0 , either with or against the direction of the B_0 field (known as the z-axis). The summated magnetic effect from all the ^1H nuclei is referred to as the equilibrium magnetization, which is excitable by a radiofrequency pulse to generate an MRI signal. The ^1H nuclei in different tissue environments (fat, complex protein, simple fluids, etc.) have characteristic frequencies. A radiofrequency pulse is designed so that it has a specific frequency that can activate the ^1H nuclei to generate a measurable MRI signal specific to the tissue. The spatial location of a ^1H nuclei is organized by three-dimensional (3D) magnetic field gradients inside the scanner. After delivery of a radiofrequency pulse, the electromagnetic energy absorbed by the ^1H nuclei will be released back to the environment by two coexisting mechanisms, longitudinal magnetization recovery and transverse magnetization decay. The rates of longitudinal magnetization recovery and transverse magnetization decay are measured by T1 and T2 (or T2*) values, respectively. They are important because MRI can use different pulse sequence designs to capture patterns of change in these rates to generate signal differences (contrast) on an image to identify tissue types, differentiate normal versus pathologic states, and quantify severity of pathophysiology at the tissue level. The choice of signal contrast weighting of the imaging method is partly dictated by the physiologic characteristics of the tissue being studied. For qualitative interpretation, signal enhancement (from T1 effects) is in general preferred in CMR, thus most pulse sequences used in CMR are T1-weighted techniques. Current common T1-weighted CMR techniques include gradient echo cine, myocardial perfusion, late gadolinium enhancement (LGE), and phase contrast blood flow imaging. T2-weighted and T2*-weighted CMR are primarily for imaging of myocardial edema and iron content, respectively. Cine steady-state free precession (SSFP), the standard pulse sequence for quantifying cardiac volumes and functions, employs a mixed T2/T1 weighting.

CONTRAST AGENTS IN CMR

Gadolinium-based contrast agents (GBCAs) are most commonly used in clinical CMR. When injected as an intravenous bolus, a GBCA transits through cardiac chambers and coronary arteries over 15 to 30 seconds

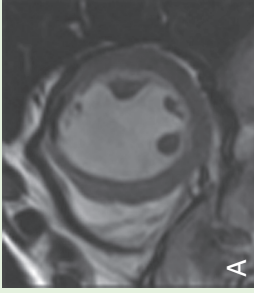
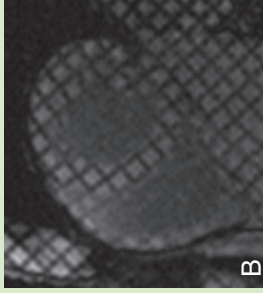
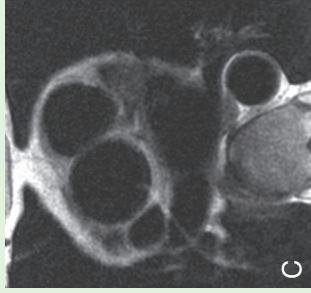
(*first-pass phase*) before it diffuses into the extracellular space. At approximately 10 to 15 minutes after injection, a transient equilibrium between contrast washing-in into the extracellular space and washing-out to the blood pool is reached. At present, myocardial perfusion CMR and most magnetic resonance angiograms (MRAs) are performed during the first-pass phase, whereas LGE images are obtained during the equilibrium phase. All GBCAs are chelated to render them nontoxic and to facilitate renal excretion. GBCA use is associated with mild reactions (nausea, mild skin rash) in ~1% and severe reactions are extremely rare. In patients with severe renal dysfunction, GBCA use may expose the patient to the toxic nonchelated free gadolinium (Gd^{3+}), which can lead to nephrogenic systemic fibrosis (NSF), an interstitial inflammatory reaction that can lead to severe skin induration, contracture of the extremities, fibrosis of internal organs, and death. Risk factors to developing NSF include estimated glomerular filtration rate (eGFR) $<30 \text{ mL/min/1.73 m}^2$, need for hemodialysis, acute renal failure, and presence of concurrent proinflammatory events. With implementation of routine screening of those at risk with creatinine clearance, weight-based dosing, avoidance of GBCA use in patients with eGFR $<30 \text{ mL/min/1.73 m}^2$, and the use of a macrocyclic form (group II) of GBCA, NSF from GBCA had a near-zero incidence globally over the past decade. In April 2020, the American College of Radiology considered the risk of NSF from group II GBCA as sufficiently low or possibly nonexistent such that questionnaire screening and eGFR testing are no longer mandatory.

CMR IMAGING METHODS

To overcome blurring from cardiac motion, data acquisition is synchronized to the electrocardiogram (ECG) signal (cardiac gating), which is either prospective (ECG triggering follows imaging data acquisition in each cardiac cycle) or retrospective (continuous data acquisition with subsequent reconstruction based on ECG timing). For cine imaging, retrospective gating is preferred because it covers the entire cardiac cycle. Many CMR pulse sequences fractionate the data acquisition of an image to occur within a narrow window of the cardiac cycle over several heartbeats (segmented approach). To overcome blurring from respiratory motion, patient breath-holding, tracking of diaphragmatic position and motion (navigator methods), averaging of respiratory motion, and combinations can be used. In patients who cannot breath-hold or have irregular heart rhythms, static single-shot and real-time cine imaging (both involve rapid acquisition of whole images within a cardiac cycle) can achieve diagnostic studies at reduced temporal and spatial resolutions. [Table 19.1](#) shows a summary of the most common clinical CMR pulse sequence techniques at our center. CMR uses bright-blood cine SSFP imaging or dark-blood fast spin-echo (FSE) imaging to assess cardiac morphology and structure. Cine SSFP can image the heart in motion at a high temporal resolution of 30 to 45 msec during a breath-hold of <10 seconds. For dark-blood techniques, T1-weighted FSE is used for morphology of cardiac chambers, vascular structures, pericardium, and imaging of fat. T2-weighted FSE with fat suppressed can image for myocardial edema. Myocardial tagging has been extensively validated to assess myocardial strain by marking the myocardium with dark lines or a grid to quantify the deformational change across the cardiac cycle. This type of intrinsic myocardial performance can be quantified global and regional in circumferential, longitudinal, and radial directions. However, the detection and tracking of tagged grids requires significant postprocessing effort and time, limiting clinical efficiency. Feature



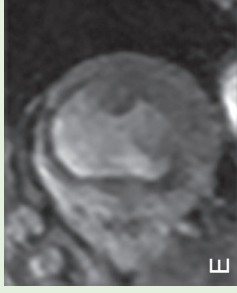
TABLE 19.1 Summary of Common Clinical Cardiac Magnetic Resonance (CMR) Pulse Sequence Techniques at Brigham and Women's Hospital

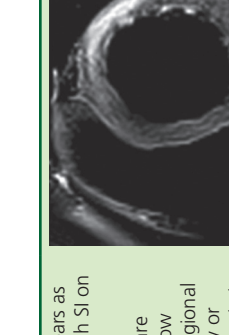
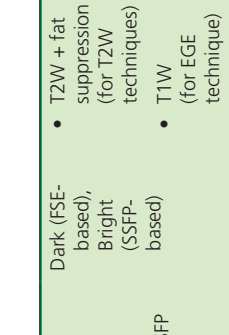
CMR TECHNIQUES	PULSE SEQUENCE OPTIONS	DARK/BRIGHT BLOOD	CONTRAST WEIGHTING	TYPICAL IN-PLANE SPATIAL/TEMP. RESOLUTIONS AND OTHER IMAGING PARAMETERS	BREATH-HOLD REQUIRED	GADOLINIUM CONTRAST REQUIRED	RELATIVE MERITS OF THE PULSE SEQUENCE OPTIONS	IMAGE EXAMPLE
Cine cardiac structure and ventricular function	<ul style="list-style-type: none"> Cine SSFP* Cine FGRE Real-time cine SSFP 	Bright	T2/T1W for cine SSFP and real-time cine SSFP; T1W for FGRE	<ul style="list-style-type: none"> 1.5-2.5 mm/~45 msec per phase Adjust number of lines of K-space per cardiac cycle (segments) to balance temporal resolution and duration of patient breath-holds 2.3-3.2mm/~60ms for real-time cine 	Yes for ECG-gated cine SSFP and FGRE. Optional for real-time cine	No	<p>Cine SSFP has higher SNR and CNR (between endomyocardium and blood) than FGRE but is sensitive to field inhomogeneity (especially at 3T), giving rise to banding artifact</p> <p>FGRE has weaker endocardial definition than cine SSFP, but it is an alternative when severe artifact exists in cine SSFP</p> <p>Good shimming or frequency scout would be needed at 3T to eliminate banding artifact</p> <p>Real-time cine SSFP: Use in patients with significant arrhythmia or difficulty breath-holding. It has the lowest spatial and temporal resolutions</p>	 <p>A</p> <p>Cine SSFP</p>
Quantitative regional myocardial strain	Myocardial tagging (newer but less widely available techniques for regional strain exist, see text)	Bright	T1W	<ul style="list-style-type: none"> Tag spacing 5-10 mm Temporal resolution ~45 msec Low flip angle, on order of 10° to limit tag fading 	Yes	No	<p>Tissue-tracking quantitation of intramyocardial motion</p> <p>Disadvantages: Tag lines fade near end of cardiac cycle and time-consuming strain analysis (postprocessing)</p>	 <p>B</p>
Structure, morphology, and fat imaging	<ul style="list-style-type: none"> Standard FSE* SS FSE (or HASTE) 	Dark	T1W ± fat suppression	<ul style="list-style-type: none"> 0.8-1.5 mm/every cardiac cycle 	Yes for standard fast SE. No for SS FSE	No	<p>Standard FSE has better image quality but relatively long scan time</p> <p>Fat suppression can be achieved by fat saturation pulse (more specific) or by suppressing tissues with short T1 (a technique known as STIR, which is less specific for fat, in particular post Gd contrast).</p> <p>SS FSE covers the whole heart quickly and is useful in patients with arrhythmia or limited breath-holding</p>	 <p>C</p>

Continued



TABLE 19.1 Summary of Common Clinical Cardiac Magnetic Resonance (CMR) Pulse Sequence Techniques at Brigham and Women's Hospital—cont'd

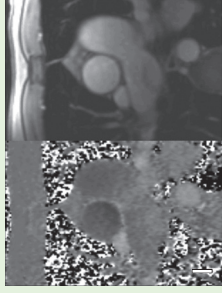
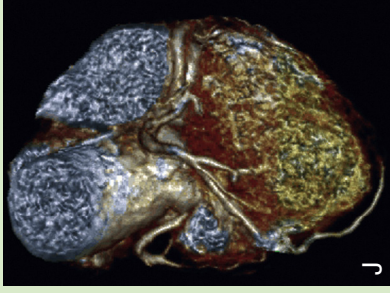
CMR TECHNIQUES	PULSE SEQUENCE OPTIONS	DARK/BRIGHT BLOOD	CONTRAST WEIGHTING	TYPICAL IN-PLANE SPATIAL/TEMP RESOLUTIONS AND OTHER IMAGING PARAMETERS	BREATH-HOLD REQUIRED	GADOLINIUM CONTRAST REQUIRED	RELATIVE MERITS OF THE PULSE SEQUENCE OPTIONS	IMAGE EXAMPLE
Myocardial scar by LGE imaging	<ul style="list-style-type: none"> Standard 2D segmented FGRE* 2D SS SSFP technique 3D whole-heart techniques (breath-hold or navigator-guided) Segmented or SS PSIR (phase sensitive image reconstruction) 	Bright or Dark (if "black-blood" LGE is used)	T1W (10-30 minutes after 0.1-0.2 mmol/kg GBCA injection)	<ul style="list-style-type: none"> 1.5-2.0 mm/150-200 msec (for standard 2D) Adjust inversion time and time delay after ECG detection to null "normal" myocardium and to image in diastole, respectively 	Yes for standard 2D technique. No for SS technique	Yes	<ul style="list-style-type: none"> Standard 2D technique has higher spatial and temporal resolutions than the SS technique 2D SS technique covers the whole heart quickly and is useful in patients with arrhythmia or difficulty breath-holding PSIR is less inversion time-sensitive and gives improved contrast when normal myocardium is not perfectly nulled New 3D application using navigator-guidance yields higher SNR than 2D and can achieve spatial resolution of <1 mm without the need for breath-holding Black-blood LGE imaging helps better identify small subendocardial scar 	 <p>D 2D segmented LGE</p>
Myocardial perfusion imaging	<ul style="list-style-type: none"> Saturation prepared gradient-echo based 2D techniques: <ul style="list-style-type: none"> - FGRE* - Hybrid GE-echoplanar (EPI) - SSFP 	Bright	T1W	<ul style="list-style-type: none"> 2.0-3.0 mm 130-180 msec per slice 3-4 locations every cardiac cycle or 6-8 locations every two cardiac cycles during vasodilator stress and rest 0.05-0.1 mmol/kg IV GBCA injected at 4 or 5 mL/sec (qualitative assessment only) 	No, but breath-hold is preferable	Yes	<ul style="list-style-type: none"> Breath-holding useful to track contrast-enhancement in specific segments Parallel-imaging acceleration and sparse sampling to reduce acquisition time per slice and extend slice coverage of the heart, but carries signal-to-noise penalty 	 <p>E</p>

Myocardial edema imaging	<ul style="list-style-type: none"> • T2W FSE* • STIR FSE • T1W EGE_r • T2 prep SSFP • T2 map 	Dark (FSE-based), Bright (SSFP-based)	T2W + fat suppression (for T2W techniques) T1W (for EGE technique)	<ul style="list-style-type: none"> • In-plane spatial and temporal resolutions similar to standard FSE • Slice thickness 7-10 mm to improve SNR • For qualitative assessment, algorithm needed to correct for the distance of the heart from the receiver surface coils is required • T2 map for quantification (insensitive to signal non-uniformity) 	Yes	No/Yes for early gadolinium enhancement (EGE) _r	<ul style="list-style-type: none"> • Myocardial edema appears as a transmural area of high SI on T2W images • In FSE techniques, beware of artifacts from slow flow especially adjacent to regional wall motion abnormality or the LV apex, which may mimic edema • Regional myocardial signal variation from phase array coils may mimic edema • In absence of LGE, T2W edema reflects reversible myocardial injury • Using T2W FSE techniques, an SI ratio of myocardium over skeletal muscle >1.9 has been reported to be abnormal in myocarditis • An EGE, between myocardium and skeletal muscle of ≥ 4 or an absolute myocardial SI increase of 45% after contrast are considered abnormal in myocarditis • The bright-blood SSFP-based technique has improved CNR and is less susceptible to slow flow artifact • T2 map is insensitive to surface coil related signal inhomogeneity and slow flowing blood-related artifact 	
Myocardial iron content imaging	T2*W multiple echo times FGRE	Bright	T2*W	<ul style="list-style-type: none"> • 2.0-3.0 mm/ ~100-150 msec • One short-axis mid-ventricular location • A series of images with 6-8 echoes that goes from ~2 to 35 msec • Axial ungated acquisition of the liver for comparison 	Yes	No	<ul style="list-style-type: none"> • Measurement is most accurate and reproducible in the mid septum • T2* value describes the exponential decay of myocardial SI as the echo time increases • At 1.5T, T2* value of <20 msec with LV dysfunction (without other obvious cause) indicates iron-overload cardiomyopathy 	

Continued



TABLE 19.1 Summary of Common Clinical Cardiac Magnetic Resonance (CMR) Pulse Sequence Techniques at Brigham and Women's Hospital—cont'd

CMR TECHNIQUES	PULSE SEQUENCE OPTIONS	DARK/BRIGHT BLOOD	CONTRAST WEIGHTING	TYPICAL IN-PLANE SPATIAL/TEMP RESOLUTIONS AND OTHER IMAGING PARAMETERS	BREATH-HOLD REQUIRED	GADOLINIUM CONTRAST REQUIRED	RELATIVE MERITS OF THE PULSE SEQUENCE OPTIONS	IMAGE EXAMPLE
Cardiac thrombus	<ul style="list-style-type: none"> LGE with long inversion time EGE imaging 	Bright	T1W	<ul style="list-style-type: none"> In-plane spatial and temporal resolutions similar to LGE imaging EGE is acquired within the first 5 min after gadolinium injection 	Yes	Yes	<ul style="list-style-type: none"> LGE imaging with inversion time set at 600 msec or longer or EGE imaging can detect thrombus indicated by an intense "black" regions Look for thrombus in locations of stagnant flows 	
Cardiac blood flow	Phase contrast imaging cine GE	Bright	Velocity-related signal phase shift	<ul style="list-style-type: none"> 1.5-2.5 mm/50 msec per phase Keep number of lines of K space per cardiac cycle (segments) low to improve temporal resolution during free breathing studies 	No (multiple signal averages used)	No	<ul style="list-style-type: none"> Multiple averages can reduce ghosting artifacts from respiratory motion during free breathing Should keep velocity encoding strength slightly > the highest expected flow velocity to avoid velocity aliasing while maximizing accuracy Background phase correction may be needed for accurate results 	
Coronary MRA	<ul style="list-style-type: none"> 3D whole heart volume using SSFP or FGRE*[†] Target-vessel approach 	Bright	T2 prepared 3D SSFP or FGRE technique	<ul style="list-style-type: none"> ~0.6-1.0 mm in-plane Free-breathing navigator-guided 3D technique is currently most widely used 	No, but yes for target-vessel approach	Yes at 3T or optional at 1.5T (no need for contrast with SSFP-based technique)	<ul style="list-style-type: none"> Compared with the target-vessel approach, 3D coronary MRA has higher SNR and provides volumetric whole-heart coverage T2-prepared SSFP sequence with suppression of the adjacent epicardial fat provides the strong blood vessel contrast Contrast-enhanced FGRE-based technique is used in 3T 	



- 3D FGRE MRA of the left atrial volume and pulmonary veins
 - Subtraction mask scan is necessary to enhance the MRA images
 - Coronal (more common) or axial 3D MRA of the entire left atrium and the pulmonary vein is generated for electrophysiologic mapping
- Use same parameters as in the subtraction mask scan

Anatomy for electrophysiologic mapping of the pulmonary vein

3D FGRE MRA

Bright

T1W FGRE

Yes

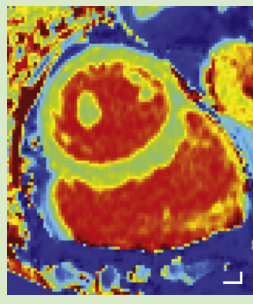
• 1.5-2.5 mm isotropic volume

• Timing bolus is required to achieve proper timing of imaging during first-pass transit of the contrast bolus

• Gating is optional but may improve border definition at the expense of prolonging breath-hold

• Free-breathing navigator-guided 3D technique is being increasingly used

Yes



- Look-Locker (LL), or modified LL 2D gradient echo
- GRE LL or SS SSFP (MOLLI)
- Varying (depending on T1)
- Yes (measurements pre- and postcontrast required)
- Yes
- 1.5-2.0 mm in-plane resolution
- LL requires complete relaxation between repetitions
- MOLLI has lower T1 resolution
- MOLLI acquires all images during single cardiac phase to allow calculation of T1 maps
- MOLLI requires SSFP read-outs
- LL can provide high T1 resolution for short T1s

T1 mapping for assessment of extracellular volume expansion and diffuse fibrosis

GRE LL or SS SSFP (MOLLI)

Varying (depending on T1)

Yes

• 1.5-2.0 mm in-plane resolution

• LL requires complete relaxation between repetitions

• MOLLI has lower T1 resolution

Yes

Yes

*More commonly used option.
 Note: Dark-blood techniques and myocardial iron content by T2* imaging should be performed before administration of gadolinium contrast.
 CMR, Contrast-to-noise ratio; EGE, early gadolinium enhancement ratio; FGRE, fast gradient-recalled echo; FSE, fast spin-echo; LGE, late gadolinium enhancement; SI, signal intensity; SMR, signal-to-noise ratio; SS, single-shot; SSFP, steady-state free precession; T1W, T1-weighted.



tracking detects and tracks the pattern of a patch of pixel of the myocardium ("feature") at blood pool-myocardial border across successive time frames. Given the feature tracking can be applied onto routine cine SSFP imaging, this application has gained increasing clinical adaptation. LGE is a T1-weighted imaging that detects accumulation of GBCA in the myocardium due to infarction, infiltration, or fibrosis. LGE is detected 5 to 15 minutes after an intravenous injection of GBCA (0.1 to 0.2 mmol/kg) (hence the term "late"). LGE data can be captured in 2D or 3D. Phase-sensitive inversion recovery (PSIR) reconstruction is routinely used in LGE imaging to enhance myocardial tissue contrast. In patients who cannot perform breath-holding, LGE imaging can be acquired using either the single-shot method or navigator guidance. CMR perfusion imaging examines the first-pass transit of an intravenous bolus of GBCA as it travels through the coronary circulation. Several perfusion techniques are available; fast bright-blood gradient-echo imaging acquires three to five short-axis slices of the heart every cardiac cycle during the injection of a GBCA bolus. Gadolinium provides strong signal enhancement in well-perfused region compared with hypoenhancement (dark regions) in poorly perfused myocardium. At a spatial resolution of approximately 2 mm in-plane, CMR perfusion can provide information of myocardial blood flow at the endocardial/epicardial or at a segmental level. T2-weighted imaging detects myocardial edema from ischemic injury or inflammation, and it has been shown to have high correlation to the area-at-risk after acute myocardial infarction (MI). It also complements LGE in determining the chronicity of an MI and allowing for accurate measurement of *salvageable myocardium*. The pulse sequence options for T2-weighted imaging include black-blood short T1 inversion recovery (STIR) FSE and the newer SSFP-type methods and their merits are listed in [Table 19.1](#). T2* is a transverse relaxation parameter well-validated method for measuring tissue iron content. A T2* of <20 msec (normal myocardium ~40 to 50 msec) is diagnostic of myocardial iron overload and a T2* of <10 msec is evidence of severe iron overload. Despite challenges from small luminal sizes and cardiac and respiratory motions, technical advances in coronary MRA imaging have favored the use of whole-heart 3D acquisition (with or without navigator guidance). Phase contrast imaging allows quantitation of velocities of blood flow and myocardial motion and intravascular flow rates. Data acquisition in MRI is slow as it acquires lines of raw data and takes approximately 200 msec to construct a single image. Parallel imaging are techniques that speed this up, using knowledge of the spatial coverage of the phased-array surface coils, to reduce the number of lines of raw data needed to be acquired by two- to threefold. It is routinely used in all commercial MRI systems to reduce acquisition time and/or improve temporal resolution. Similarly, by taking advantage of the correlation between images at different times (either within or between cardiac cycles), methods that reconstruct images at a higher efficiency using a reduced number of data (known as k-t accelerated imaging) have been in routine clinical use.

T1 and T2 Mapping

T1 mapping estimate in quantitative terms the expansion of the extracellular space in the myocardium where GBCA distribute. This method has demonstrated good correlation with collagen content of the interstitial space in conditions where diffuse fibrosis or infiltration occurs and can serve as a noninvasive method in monitoring disease progression or treatment response. Using both pre- and postcontrast T1 measurements, one determines the change of R1 ($=1/T1$) between pre- and postcontrast states in myocardium relative to the change of R1 in blood. This ratio estimates the tissue volume fraction filled by extracellular GBCA. Compare to T1-weighted imaging such as LGE, T1 mapping provides quantitation of the spectrum of extracellular volume (ECV) expansion from fibrosis or infiltration. T1 mapping techniques characterized myocardial pathology not visible by LGE imaging. Myocardial T2 mapping, which involves acquisition of a series of images with different T2 weighting, provides a quantitative measurement of regional fraction of free water in the myocardium. Compared to T2-weighted imaging, T2 mapping renders the detection of myocardial edema more reliable and is less prone to artifacts due to either motion or arrhythmia.

Patient Safety in CMR

U.S. Food and Drug Administration (FDA)-approved MRI-conditional pacemakers and implantable cardioverter defibrillators (ICDs), that allow patients to safely undergo a MRI under specific imaging settings, are now widely available. With a standard procedure of device interrogation before and after the MRI scanning established, patients with pacemakers and ICDs that are not MRI-conditional ("legacy" devices) are now routinely undergoing CMR in many experienced centers. In a series of 1509 patients with a legacy device who underwent 2103 MRI

studies, device reset was noted in 0.4%, with only one case of post-MRI device dysfunction needing replacement.¹ Sternal wires, mechanical heart valves, annuloplasty rings, coronary stents, non-metallic catheters, and orthopedic or dental implants are also safe under usual clinical CMR scanning. Common hazardous implants include cochlear implants, neurostimulators, hydrocephalus shunts, metal-containing ocular implants, most breast tissue expanders, or metallic cerebral aneurysm clips. Claustrophobia has become uncommon with the use of wide-bore scanners (~2% of patients) and most can be managed with oral sedation administered before scanning.

CLINICAL APPLICATIONS OF CMR

Coronary Artery Disease

Assessing Stable Chest Pain Syndromes

Collective evidence from the past decade demonstrated that vasodilating stress CMR perfusion imaging is accurate in diagnosing and risk stratifying for CAD in patients with stable chest pain syndromes. Stress CMR perfusion has fewer artifacts, is free from ionizing radiation, and has threefold higher spatial resolution than single-photon emission computed tomography (SPECT) (see [Chapter 18](#)). Several studies had reported that stress CMR perfusion has excellent accuracy in detecting single or multivessel coronary disease, which is higher than SPECT² ([Fig. 19.1](#) and [Video 19.1](#)). The physiologic significance of stress CMR complements sensitive assessment of coronary atherosclerosis by calcium scoring (see [Chapter 20](#)).³ Annualized cardiac event rates in patients with stable chest pain syndromes who had a negative stress CMR are consistently low across numerous single and multicenter studies.⁴ In a recent multicenter registry study of 2349 patients, patients with a negative stress CMR experienced cardiac events in 0.6% annually during 5 years of follow-up⁵ ([Fig. 19.2](#)). The use of stress CMR in this setting had been found to be cost-effective.⁶ Quantitative stress CMR perfusion using automated algorithms is becoming the standard of care in some experienced CMR centers, with its potential advantages over qualitative methods in minimizing reader's bias, assessing microvascular coronary disease ([Fig. 19.3](#)), and improving diagnostic accuracy especially in cases of possible multivessel coronary artery disease (CAD)⁷ ([Fig. 19.4](#) and [Video 19.2](#)) and prognosticating of adverse cardiac events.⁸ Multiple clinical studies and a meta-analysis had demonstrated excellent correlation of stress CMR perfusion against invasive measurement of fractional flow reserve (FFR), showcasing its high accuracy in determining the physiologic significance of coronary stenosis. In a recent randomized trial of patients with stable angina, a stress CMR strategy led to a lower incidence of coronary revascularization than invasive FFR but was noninferior in cardiac outcomes.⁹ Dobutamine stress CMR captures change in both regional cine function and perfusion. It is less often used than vasodilating stress CMR perfusion imaging as it is often reserved for patients who have a contraindication to receiving vasodilating stress infusion but nonetheless demonstrated excellent sensitivity and specificity in detecting CAD regardless of the presence of underlying resting wall motion abnormality. Multiple clinical studies have shown that dobutamine cine CMR provides strong prognostic value in risk assessment of patients. In a few specialized centers, stress CMR with exercise treadmill stress has shown promising results.¹⁰

CMR Assessment of Myocardial Viability and Benefit from Coronary Revascularization

CMR offers multicomponent assessment of structure and physiology to inform about myocardial viability (see [Chapter 36](#)). A combined criteria of end-diastolic wall thickness of >5.5 mm and cine systolic wall thickening of >2 mm has sensitivity and specificity between 85% and 90% in the prediction of segmental contractile recovery after revascularization. In addition, the transmural extent of myocardial scar detected by LGE imaging accurately depicts a progressive stepwise decrease in functional recovery despite successful coronary revascularization, especially robust in myocardial regions of akinesia or dyskinesia. LGE is easy to perform and interpret, and a 50% transmural cutoff is sensitive in detecting segmental contractile recovery. On the other hand, low-dose dobutamine cine imaging can provide a physiologic assessment of the mid-myocardial and subepicardial contractile

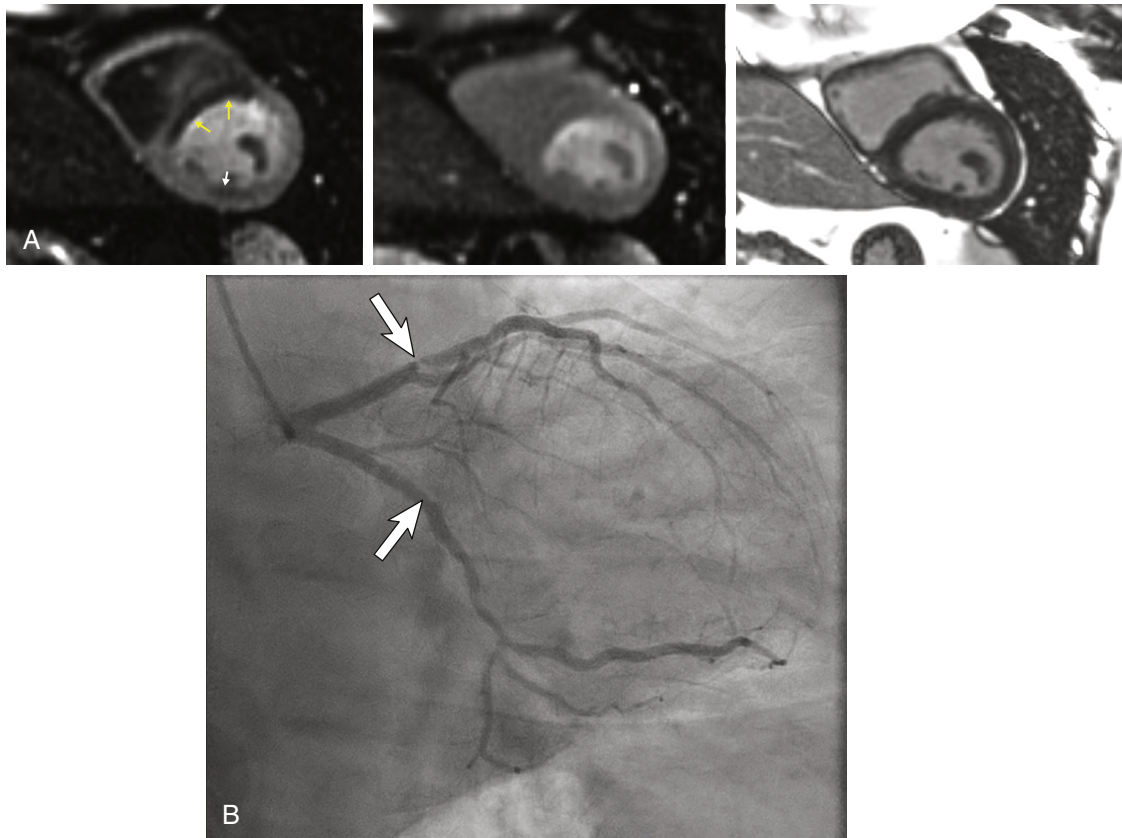


FIGURE 19.1 Stress CMR assessment of myocardial ischemia. **A**, Stress CMR perfusion (left) in a patient with intermittent chest pain shows severe hypoperfusion in the basal to mid septum (yellow arrows) and the inferolateral wall (white arrow). These defects appear reversible as no significant perfusion defect is seen at rest (middle), and the myocardium appears viable without LGE (right). **B**, Coronary angiography demonstrates severe proximal left anterior descending stenosis and moderate left circumflex stenosis. Video 19.1 displays the full imaging datasets.

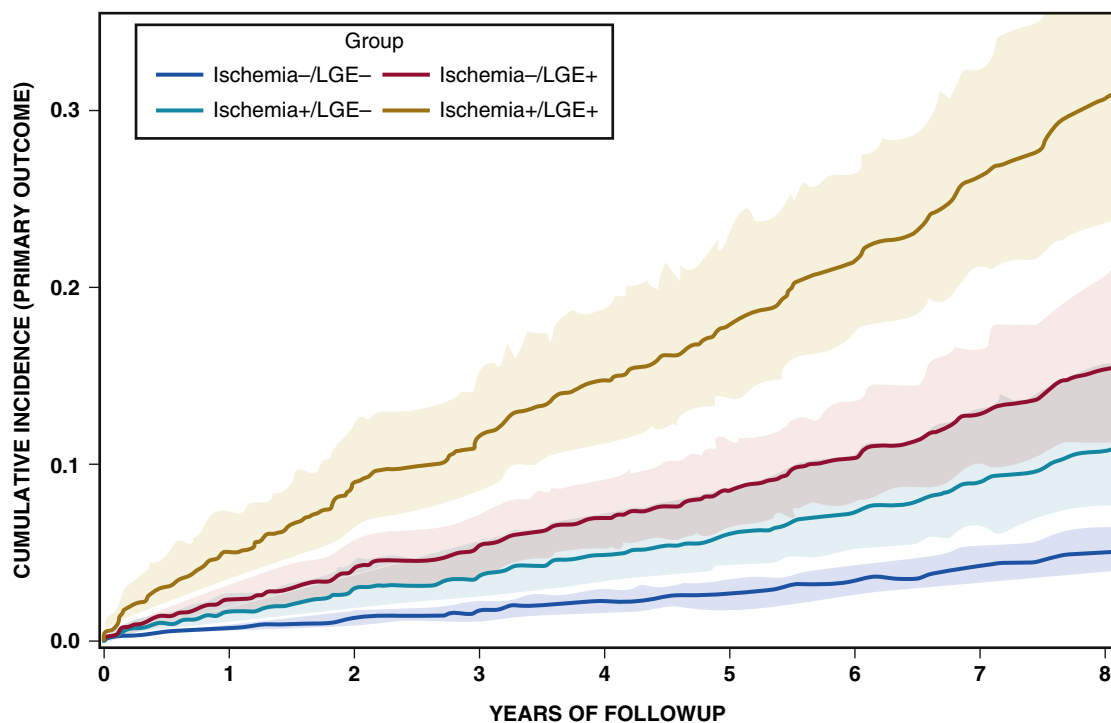


FIGURE 19.2 Stress CMR and cardiac outcome. Cumulative incidence function for the primary outcome of cardiac death or nonfatal MI in a multicenter cohort of 2349 patients presenting with stable chest pain syndromes. Patients with no ischemia (by qualitative CMR perfusion analysis) and no LGE evidence of infarction had very low incidence of primary outcome during study follow-up. (From Kwong RY, et al. Cardiac magnetic resonance stress perfusion imaging for evaluation of patients with chest pain. *J Am Coll Cardiol* 2019;74:1741-1755.)

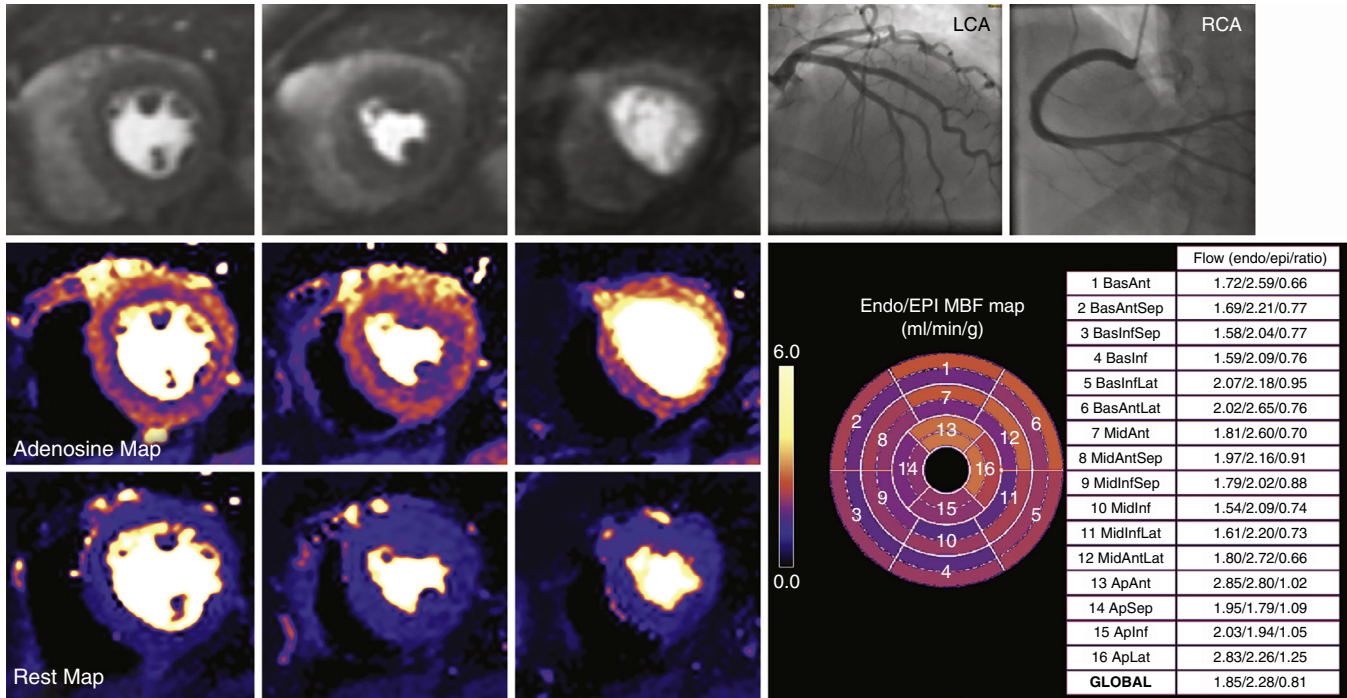


FIGURE 19.3 Microvascular coronary disease. Adenosine CMR perfusion exam in a woman with diabetes mellitus, hypertension, exertional chest discomfort, and normal coronary arteriogram reveals a diffuse subendocardial defect, prominent at the basal and mid-levels, best seen on quantitative perfusion maps. Myocardial blood flow quantification demonstrates a gradient across the myocardial wall with flow values lower in the subendocardium than the epicardium, consistent with small vessel ischemia. (Images courtesy Peter Kellman, PhD; W. Patricia Bandettini, MD.)

reserve and may be useful when tissue edema is prominent (e.g., early after an acute coronary syndrome), making infarct transmural assessment challenging.

Assessing Acute Coronary Syndromes

In a single session, MR assesses the spectrum of myocardial changes from an acute coronary syndrome using cine cardiac structure and function, myocardial perfusion, LGE imaging of infarction, and T1- or T2-weighted or mapping of myocardial edema or other tissue characteristics. At a spatial resolution of 1.5 to 2 mm and a high contrast-to-noise ratio, CMR LGE imaging is at present the most sensitive and accurate imaging method in detecting subendocardial infarction and quantifying infarct size, respectively. CMR is not indicated as a routine first-line imaging after an acute MI, but it is useful in assessing the most common issues after an acute MI, including addressing the perfusion status of MI or the extent of noninfarct salvageable myocardium, or complications such as formation of aneurysm, intracavitary thrombus, microvascular obstruction (Fig. 19.5), pericarditis, or ventricular septal defect (Fig. 19.6). In patients with an acute reperfused MI, regions of ischemic area-at-risk, microvascular obstruction (no-reflow), and intramyocardial hemorrhage can be quantified by T1 or T2 mapping, LGE, and T2* mapping, respectively. Dark-blood LGE imaging improves the detection of subendocardial infarction by enhanced discrimination of the infarct-blood border¹¹ (Fig. 19.7). In a small randomized clinical trial of patients with acute non-ST elevation MI, CMR in conjunction with coronary computed tomographic angiography (CTA) as a combined first-line approach reduced the utilization of invasive angiography without adversely affecting outcome when compared with routine care.¹² CMR is the noninvasive gold standard for infarct size and microvascular obstruction. Not only do these CMR measurements contribute to long-term prognosis after MI,¹² but they allow identification of potential benefits associated with new cardioprotective strategies both in experimental and clinical trials.¹³ In patients presenting with a ST-segment elevation myocardial infarction (STEMI) after a primary percutaneous coronary intervention (PCI), CMR has also shown moderate-good agreement with invasive FFR assessment of the significance of nonculprit coronary lesions.¹⁴

CMR is effective in diagnosing and guiding the management of acute chest pain syndromes. In a randomized study of acute chest pain patients with elevated troponins, a combined CMR and coronary CTA strategy imaging for infarction, myocardial salvage, and coronary stenosis resulted in more efficient utilization of invasive coronary angiography.¹⁵

In a cohort of 388 patients with acute elevation of serum troponins but with nonobstructive coronary arteries, CMR identified the causes for abnormal troponins in approximately three-fourths of patients as myocarditis, acute MI, or other cardiomyopathies. The remaining one-fourth with no abnormality on CMR had a favorable prognosis.¹⁶ In a recent study of 229 patients with elevated troponins and nonobstructed coronary arteries, the use of a new 3D free-breathing (navigator-prepped) LGE imaging method enabled an in-plane resolution of 1.3 mm in infarct detection and reduced inconclusive diagnosis by 29%¹⁷ (Fig. 19.8 and Video 19.3).

Cardiomyopathies

Overall Approach to Undiagnosed Cardiomyopathy

CMR is an invaluable tool for assessing various cardiomyopathies given its multifaceted interrogation of ventricular structure and myocardial physiology in matching arbitrary scan planes. CMR assessment of rest and stress myocardial perfusion, regional function, LGE, and T2-weighted imaging is useful in differentiating causes of cardiomyopathies and providing guidance for management. In the past few years, T1, ECV fraction, and other tissue mapping methods have provided novel diagnostic insights and validated noninvasive estimates of severity of fibrosis or infiltration from various causes of cardiomyopathy.¹⁸ Inclusion of a stress CMR component is complementary to LGE imaging of infarction in ruling out ischemia as a factor in cardiomyopathy. Multiple multinational registries now exist with CMR incorporated to advance the understanding of the interacting roles of genotypes and risks in patients in various forms of genetic cardiomyopathies.¹⁹ The presence, pattern, and extent of LGE continue to demonstrate strong prognostic association with serious ventricular arrhythmias and sudden cardiac death in various types of cardiomyopathies, although specific guidance of ICD therapies is a matter of ongoing research.²⁰

Hypertrophic Cardiomyopathy

Compared with echocardiography, CMR provides a more complete 3D morphologic pattern of left ventricular (LV) hypertrophy and tissue characteristics in patients with hypertrophic cardiomyopathy (HCM) and can monitor the progression of disease at a higher precision than echocardiography (see Chapter 16).²¹ CMR has higher sensitivity than

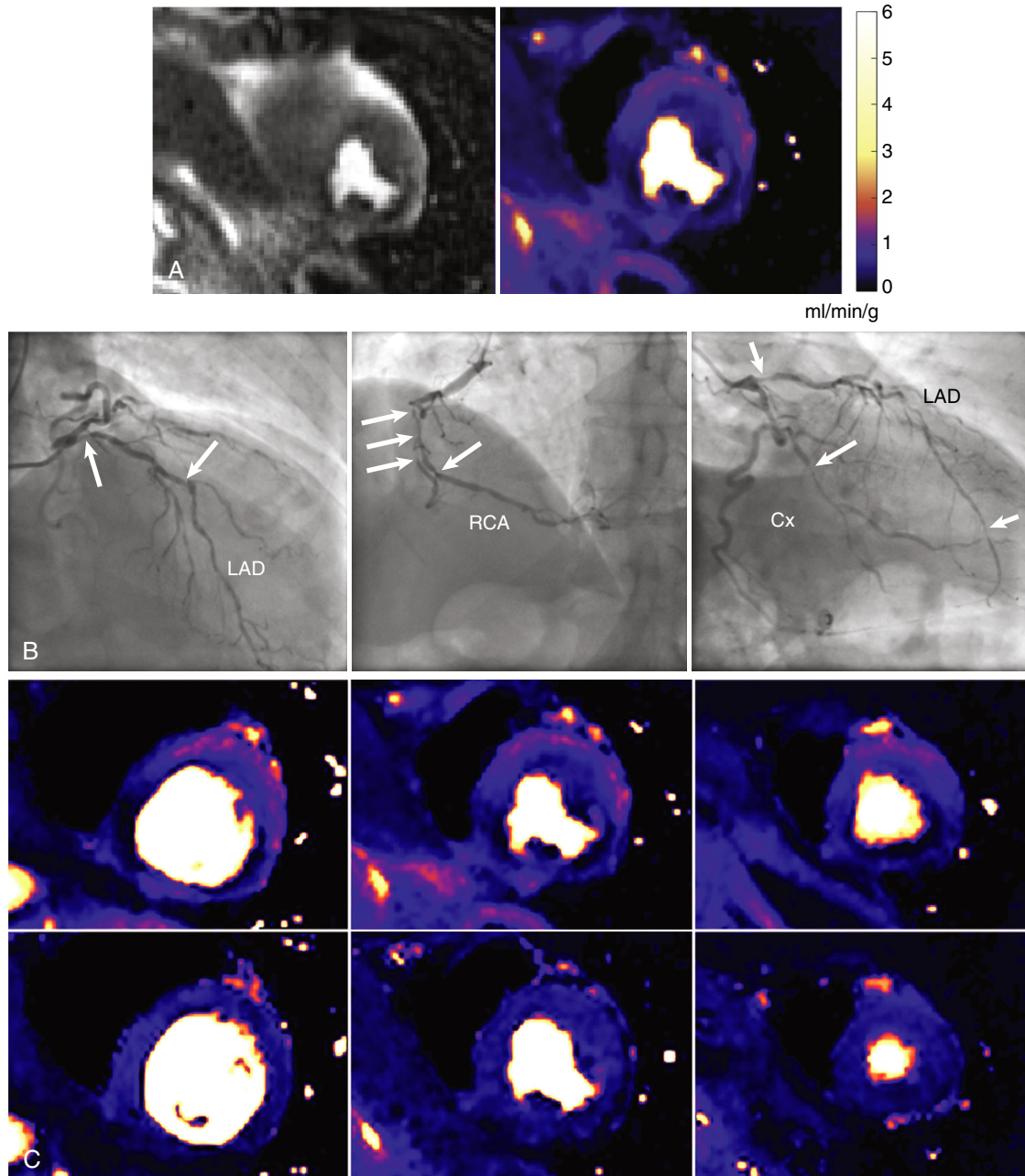


FIGURE 19.4 Quantitative CMR perfusion mapping in multivessel CAD. **A**, First-pass adenosine stress perfusion image (left) and corresponding quantitative myocardial perfusion map (right) in a patient with angiographically confirmed unbalanced three-vessel CAD (**B**). Visual analysis suggested discrete stress perfusion defects whereas perfusion maps show more extensive global ischemia consistent with three vessel disease (**C**). See Video 19.2. (Images courtesy Peter Kellman, PhD, NIH, Bethesda, MD, USA and Drs. Tushar Kotecha and Marianna Fontana, Royal Free Hospital, London, UK.)

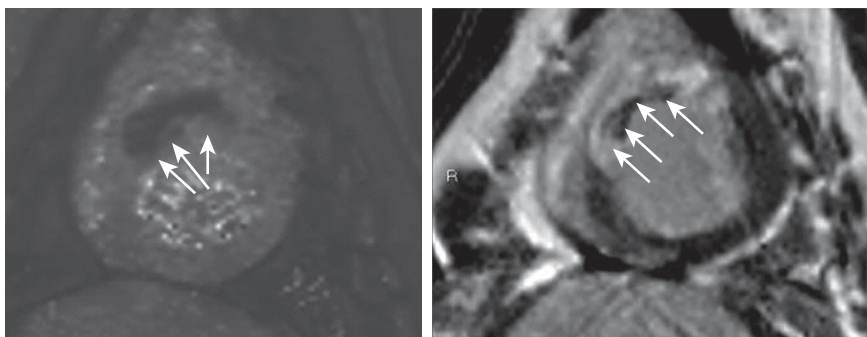


FIGURE 19.5 Microvascular obstruction. **Left**, Short-axis T2*-weighted image from a porcine model of reperfused MI demonstrating intramyocardial hemorrhage in the anteroseptum. **Right**, Short-axis phase-sensitive inversion recovery LGE image in the same animal demonstrating transmural LGE with a mid-wall region of intramyocardial hemorrhage. (Courtesy Christopher Kramer, MD and Michael Salerno, MD, PhD, University of Virginia Health System.)

echocardiography for diagnosing HCM by capturing hypertrophy of the basal anterior wall or apical aneurysm, which are occasionally missed by echocardiography (Fig. 19.9 and Videos 19.4 and 19.5). LV mass index varies widely with maximal LV wall thickness due to heterogeneity of the HCM phenotype (see Chapter 54). Markedly elevated LV mass index (men >91 g/m² and women >69 g/m²) and maximal wall thickness of >30 mm have been shown to be sensitive and specific markers of risk of cardiac death, respectively. In a large series, the extent of LGE was indicative of heterogeneous fibrosis and was associated with ventricular arrhythmias, progressive LV dilation, and cardiac events, regardless of presence of out-flow obstruction or prior septal myectomy.²² The

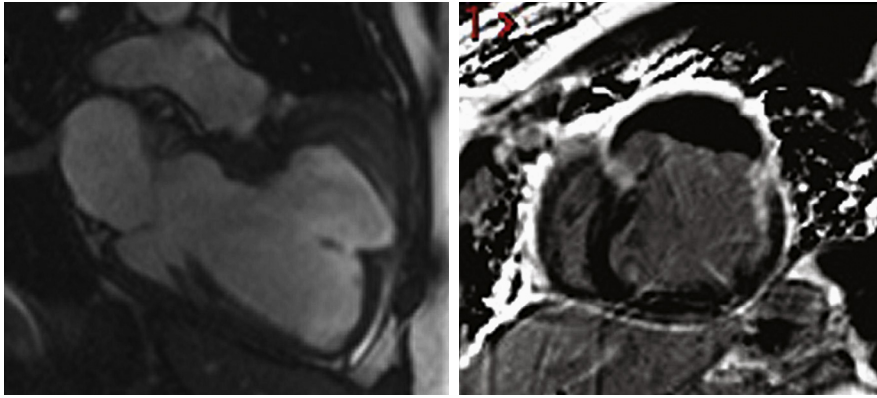


FIGURE 19.6 Ventricular pseudoaneurysm. **Left**, A two-chamber long-axis SSFP cine image at end-diastole in a patient 5 years after anterior MI demonstrating a chronic anterior pseudoaneurysm. Note the narrowed neck of the pseudoaneurysm. **Right**, Short-axis phase-sensitive inversion recovery LGE image from the same patient demonstrating enhancement of the fibrous outer layer of the pseudoaneurysm, which is lined with thrombus, which appears black. (Courtesy Christopher Kramer, MD and Michael Salerno, MD, PhD, University of Virginia Health System.)

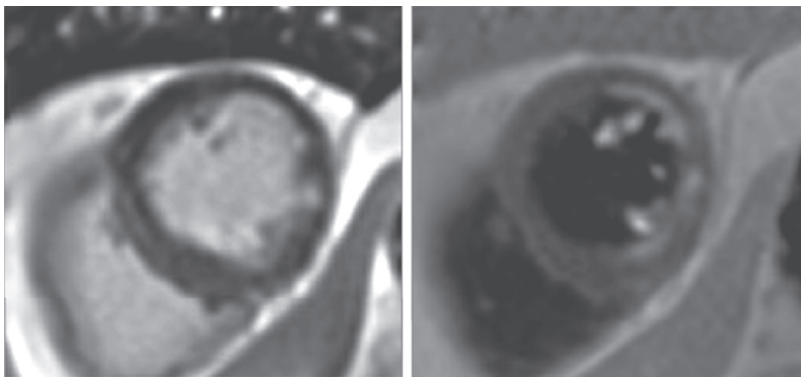


FIGURE 19.7 Dark-blood LGE. Dark-blood LGE imaging increases the contrast between endocardial infarction and blood pool, which allows better delineation of the subendocardial infarct border and increased sensitivity in infarct detection. (Courtesy Peter Kellman, PhD, NIH, Bethesda, MD, USA.)

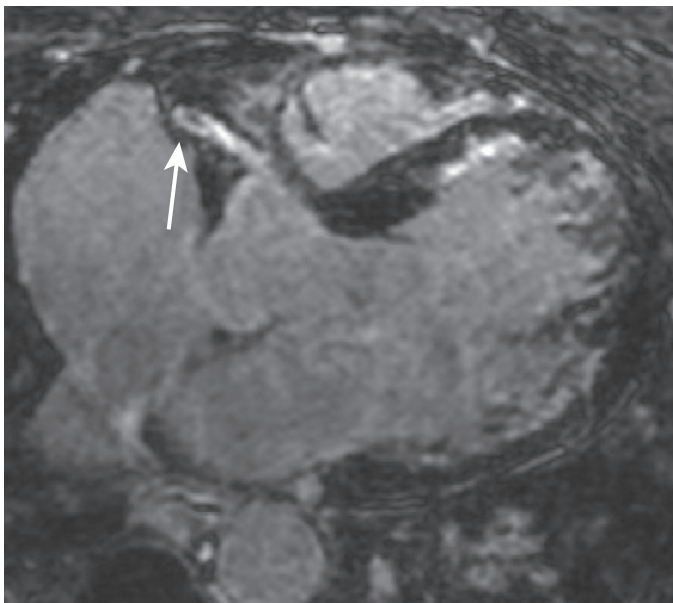


FIGURE 19.8 High resolution 3D late gadolinium enhancement. A free-breathing 3D CMR dataset that captures both coronary anatomy (*arrow*) and an anteroseptal and apical myocardial infarction. Compressed sensing data acquisition and reconstruction were used to shorten the scan time. See Video 19.3. (Courtesy Reza Nezafat, PhD, Beth Israel Deaconess Medical Center.)

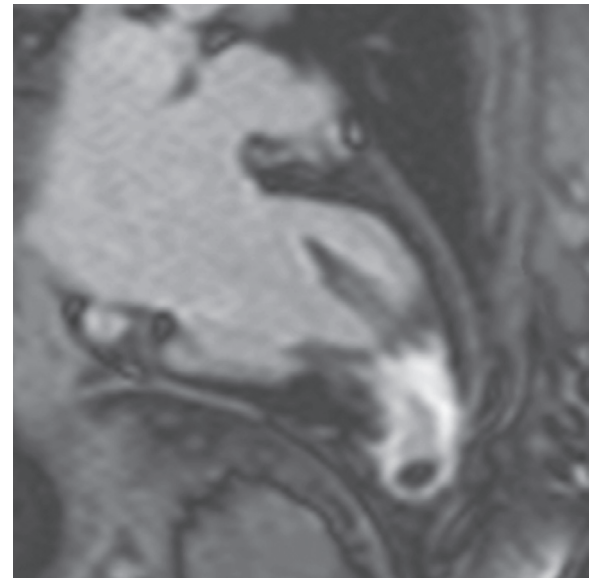


FIGURE 19.9 Apical hypertrophic cardiomyopathy with apical thrombus. CMR in a 36-year-old man with syncope demonstrates “burnt out” apical HCM with evidence of an apical LV thrombus on LGE imaging and cine functional four- and two-chamber imaging (Video 19.4 and 19.5, respectively). The apical thrombus resolved with anticoagulation and an ICD was implanted. (Courtesy Naeem Merchant, MD and Bobak Heydari, MD, MPH, Stephenson Cardiac Imaging Center, University of Calgary, Calgary, Canada.)

multifaceted approach by CMR allows an individualized characterization of abnormal myocardial pathophysiology secondary to coronary microvascular dysfunction, fibrosis, and hypertrophy. Quantifying left atrial remodeling by cine CMR, LGE, and regional strain imaging estimates the risk of atrial fibrillation in HCM patients.²³ Recent work from specialized centers demonstrated that in vivo myocardial disarray could be imaged by diffusion tensor CMR. The directionality of myocardial disarray (known as fractional anisotropy) was shown to have strong association with ventricular arrhythmia independent of presence of fibrosis.²⁴ A National, Heart, Lung, and Blood Institute (NHLBI)-funded prospective multinational registry (HCMR) has recently completed enrollment of 2755 HCM patients incorporating CMR, genetic data, biomarker data, and clinical outcomes.²⁵ On the other hand, CMR has also been included in the large international Sarcomeric Human Cardiomyopathy Registry (SHaRe) describing long-term national history of HCM patients with LV dysfunction.²⁶

Arrhythmogenic Cardiomyopathy

Arrhythmogenic cardiomyopathy distinguishes itself from other cardiomyopathies by (1) a predisposition toward ventricular arrhythmia that precede overt morphologic abnormalities and even histologic substrate and (2) diverse phenotypic manifestations including LV or biventricular involvement (see [Chapter 52](#)). CMR offers advantages over echocardiography by its quantitative and volumetric assessment of right ventricular (RV) function and its fibrofatty tissue characterization of myocardium. The 2010 Task Force Criteria affirmed CMR as an integral and a standardized component in the workup of arrhythmogenic cardiomyopathy, in which it described a combination of regional RV akinesia/dyskinesia/dyssynchronous contraction and significant RV dilation or dysfunction as constituting major diagnostic criteria. These abnormalities are typically observed in predilection

areas, including the subtricuspid region, basal RV free wall, and LV posterolateral wall.²¹ Evidence of RV fat by CMR as an isolated finding is of limited diagnostic specificity, but fat-suppressed LGE imaging of the RV fibrosis has shown a high correlation with endomyocardial biopsy and the inducibility of ventricular arrhythmias. In a recent cohort of 140 patients with a definite diagnosis of arrhythmogenic cardiomyopathy who were followed for 5 years, biventricular, isolated LV and isolated RV involvement were reported in 37%, 12%, and 41%, respectively. Patients with LV involvement experienced substantially higher risk of sudden death or arrhythmic events than those with solitary RV involvement, and no events were observed in those with a negative CMR²⁷ (Fig. 19.10 and Video 19.6).

Myocarditis

CMR targets the three main pathophysiologic components of myocarditis (see Chapter 55): myocardial edema by T2-weighted imaging, regional hyperemia and capillary leak by early gadolinium enhancement ratio (EGE_r), and myocardial necrosis or fibrosis by

LGE imaging. From the Lake Louise Criteria Guideline using pooled data of the single-center studies, T2-weighted imaging, EGE_r, and LGE have individual sensitivities and specificities of 70% and 71%, 74% and 83%, and 59% and 86%, respectively. A combined approach using T2-weighted images and LGE provides high diagnostic accuracy for acute myocarditis. However, two recent meta-analyses found that T1 or T2 mapping increased diagnostic accuracies over the conventional Lake Louise diagnostic criteria.^{28,29} The subepicardium and midmyocardium of the inferolateral walls have been described in parvovirus-related cases, whereas septal involvement has been associated with human herpesvirus 6 with potentially more serious sequelae. T2 mapping has been shown to differentiate acute versus healed stages of myocarditis in cases where chronicity of myocarditis is uncertain.³⁰ Several large single-center studies have indicated LGE pattern to be a strong prognostic marker,^{31,32} and monitoring of LGE changes may identify a higher risk cohort than captured by serum troponins or inflammatory biomarkers^{33,34} (Fig. 19.11 and Videos 19.7 and 19.8).

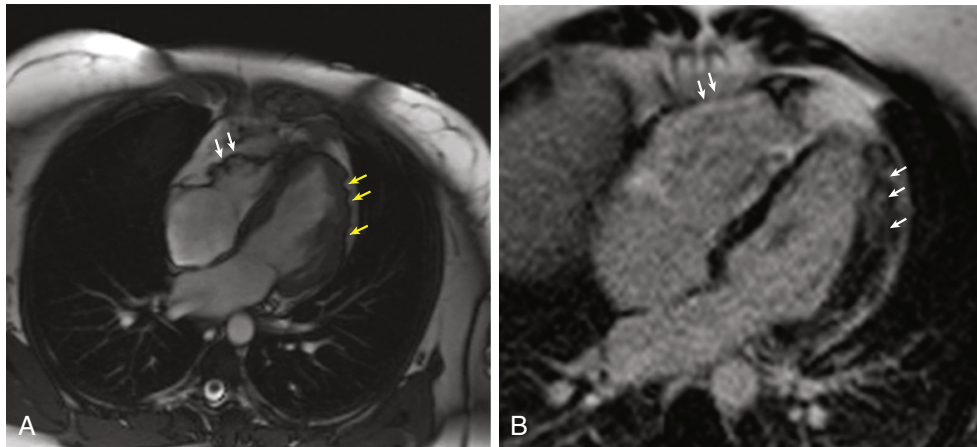


FIGURE 19.10 Arrhythmogenic cardiomyopathy. CMR images in a woman who developed heart failure following birth of her second child. The ECG showed left anterior fascicular block and frequent ventricular couplets. Echocardiography demonstrated mild LV and RV dysfunction, with hyperdynamic function of the RV apex relative to the rest of the right ventricle (McConnell's sign). The differential diagnosis included peripartum cardiomyopathy, pulmonary embolism, myocarditis, arrhythmogenic cardiomyopathy, and cardiac sarcoidosis. **A**, End-systolic frame from cine CMR (see also Video 19.6) shows "crinkling" or "accordion sign" of the RV base (white arrows) and notching of the LV epicardium due to fatty infiltration (yellow arrows). **B**, Post-contrast T1-weighted inversion recovery image shows LGE of the RV free wall and LV epicardium (arrows). These findings are highly suggestive of arrhythmogenic cardiomyopathy. Subsequent genetic testing revealed pathogenic mutations in PKP2 and Asn557Asp, confirming this diagnosis. (Courtesy Amit Patel, MD, University of Chicago Medicine.)

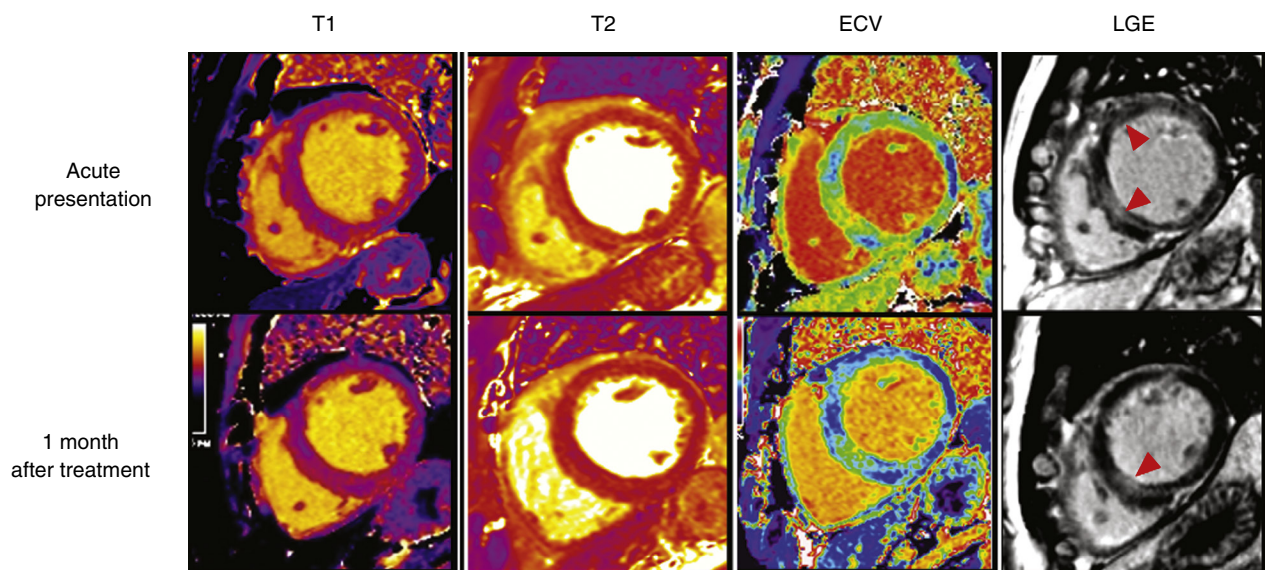


FIGURE 19.11 Serial assessment of myocarditis. **Top**, CMR at 1.5T in a 54-year-old man with fever, chills, rash, and elevated troponin, sedimentation rate, and C-reactive protein revealed dilated cardiomyopathy with a LV ejection fraction of 28% (see Video 19.7). There were diffuse inflammatory abnormalities with T1 >1300 msec, T2 >70 msec, ECV ~50%, and patchy mid-wall enhancement on LGE imaging, consistent with acute myocarditis. He was treated with intravenous immunoglobulin, methylprednisolone, tofacitinib, and tocilizumab. **Bottom**, Serial CMR aided in monitoring response to therapy, demonstrating reduction in T1 to 1100 ms, T2 to 55 ms, ECV to ~40%, and extent of LGE, as well as improvement, but not normalization, in LV volume and ejection fraction (39%) (see Video 19.8). (Courtesy Drs. W. Patricia Bandettini and Alessandra Brofferio, National Heart, Lung, and Blood Institute, Bethesda, Maryland.)

Cardiac Sarcoidosis

CMR may enhance disease detection through the successive histologic stages of disease: tissue edema, noncaseating granulomatous infiltration, and patchy myocardial fibrosis (see [Chapter 52](#)). LGE imaging has been reported to identify myocardial abnormalities due to sarcoidosis at a higher sensitivity than the modified Japanese Ministry of Health guidelines. Most commonly, cardiac infiltration based on LGE imaging is seen in multiple locations involving the septum and basal anterior part of the right ventricle. Typical cases demonstrate expansion of the wall thickness matched with LGE infiltration and occasionally high signal on T2-weighted imaging indicative of edema ([Fig. 19.12](#)). In cases where septal LGE is seen, CMR may also guide sampling during endomyocardial biopsy and increase tissue yield. In a recent cohort of 321 patients with biopsy-proven systemic sarcoidosis, CMR had higher sensitivity in screening for cardiac involvement than echocardiography. During follow-up, LGE presence portended a near sixfold increased risk of adverse cardiac outcomes, whereas echocardiographic parameters were not predictive.³⁵ In patients with known cardiac sarcoidosis, current evidence suggests that presence, multiple foci, extent of LGE, RV systolic dysfunction, and RV LGE are the strongest risk markers for mortality or significant ventricular arrhythmias.^{36,37} Per current American College of Cardiology (ACC)/American Heart Association (AHA) guideline, patients with cardiac sarcoidosis, the presence of LGE is a Class IIa indication for ICD therapy in patients with an expected meaningful survival >1 year.³⁸

Cardiac Amyloidosis

In patients with cardiac amyloidosis (see [Chapter 53](#)), CMR typically demonstrates morphologic changes of a restrictive cardiomyopathy, circumferential and diffuse LGE in the LV with possible RV subendocardial

involvement, and in some cases microvascular dysfunction on first-pass perfusion matching the LGE regions. Its diagnostic accuracy is excellent in published series and may obviate the need for endomyocardial biopsy ([Fig. 19.13](#); see also [Fig. 72.13F, G](#)). Cardiac amyloidosis from ATTR appears to show more ventricular remodeling of increased myocardial mass, transmural LGE, and RV involvement than the AL subtype, although these patterns overlap in a minority of patients. Myocardial T2 consistent with edema is highest in untreated cases and appears to reflect response to chemotherapy.³⁹ Both native myocardial T1 and ECV are increased from amyloid protein of either AL or ATTR subtypes. The transmural and extent of LGE represent advanced cardiac amyloidosis, and these findings are associated with patient mortality incremental to common risk markers including systolic and diastolic function. However, myocardial ECV quantitation has become a part of the standard diagnostic algorithm because it offers a more complete quantitation of the regional and global severity of amyloid infiltration as well as in monitoring treatment response. Multiple studies and a recent meta-analysis demonstrated that ECV provided incremental diagnostic and prognostic values over LGE and native T1.⁴⁰ Patients with the uncommon cardiomyopathy secondary to hypereosinophilic syndromes may mimic amyloidosis on echocardiography but have characteristic features on CMR including diffuse endocardial fibrosis and mural thrombi ([Fig. 19.14](#) and [Videos 19.9 and 19.10](#)).

Idiopathic Dilated Cardiomyopathy

CMR in idiopathic dilated cardiomyopathy (see [Chapter 52](#)) can rule out ischemic or myocardial infiltration as cause of cardiomyopathy, detect patterns of LGE (which have diagnostic and prognostic values), and monitor treatment response and disease progression. Current

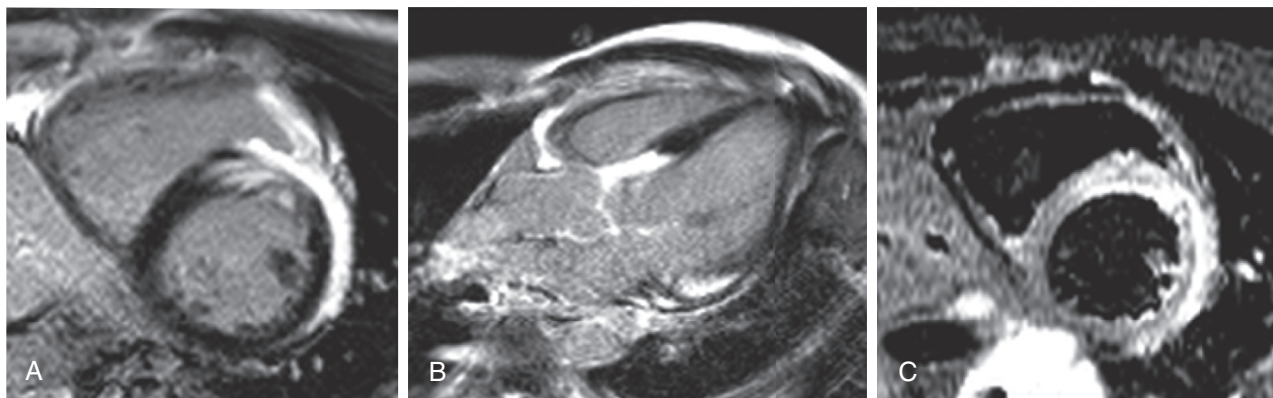


FIGURE 19.12 Cardiac sarcoidosis. CMR in a 48-year-old woman with new-onset complete heart block and history of pulmonary sarcoidosis demonstrated extensive LV subepicardial late gadolinium enhancement in short axis (**A**) and long axis (**B**) images, consistent with cardiac involvement, and myocardial edema on T2-weighted imaging suggesting active inflammation (**C**). Intravenous pulse steroids resulting in resolution of the heart block. (Courtesy Naeem Merchant, MD and Bobak Heydari, MD, MPH. Stephenson Cardiac Imaging Center, University of Calgary, Calgary, Canada.)

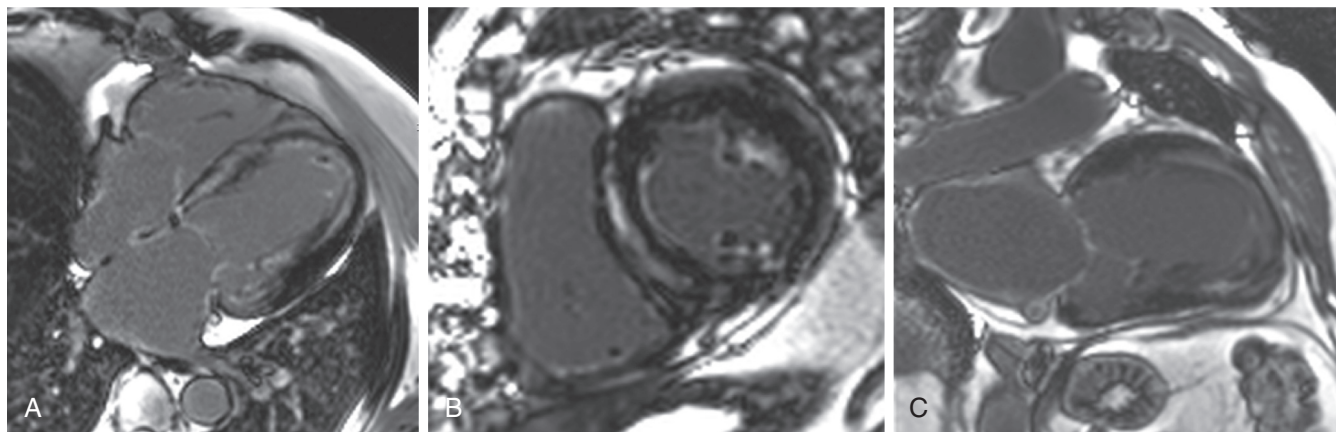


FIGURE 19.13 Cardiac amyloidosis. CMR in a 75-year-old man with worsening heart failure with persevered ejection fraction demonstrated extensive mid-wall LV (**A** and **B**) and left atrial (**C**) LGE consistent with cardiac amyloidosis. Subsequent RV biopsy confirmed the diagnosis of transthyretin (ATTR) amyloidosis. (Courtesy Naeem Merchant, MD and Bobak Heydari, MD, MPH. Stephenson Cardiac Imaging Center, University of Calgary, Calgary, Canada.)

evidence indicates that in absence of infarct LGE or perfusion abnormality, ischemic causes of LV dysfunction can be excluded (Fig. 19.15 and Video 19.11). This gatekeeper approach has been robust in most experienced CMR centers, where many patients can be spared the procedural risk, efforts, and costs of an invasive angiography. In about 30% of patients with idiopathic dilated cardiomyopathy, a patch or linear mid-wall striate septal LGE has been reported and its extent is associated with a lack of response to medical therapy, sudden death,

and inducible ventricular tachycardia, independent of LV size and function.⁴¹ ECV mapping has been validated histologically, and it has been shown that a diffuse extent of fibrosis is a stronger marker for heart failure outcomes than LGE.¹⁸ Currently in investigation, the use of feature tracking and myofiber orientation appear promising to better understand of cardiac mechanics toward heart failure outcome,^{42,43} whereas novel tissue characterization may allow better understanding of arrhythmic risks in this condition.⁴⁴

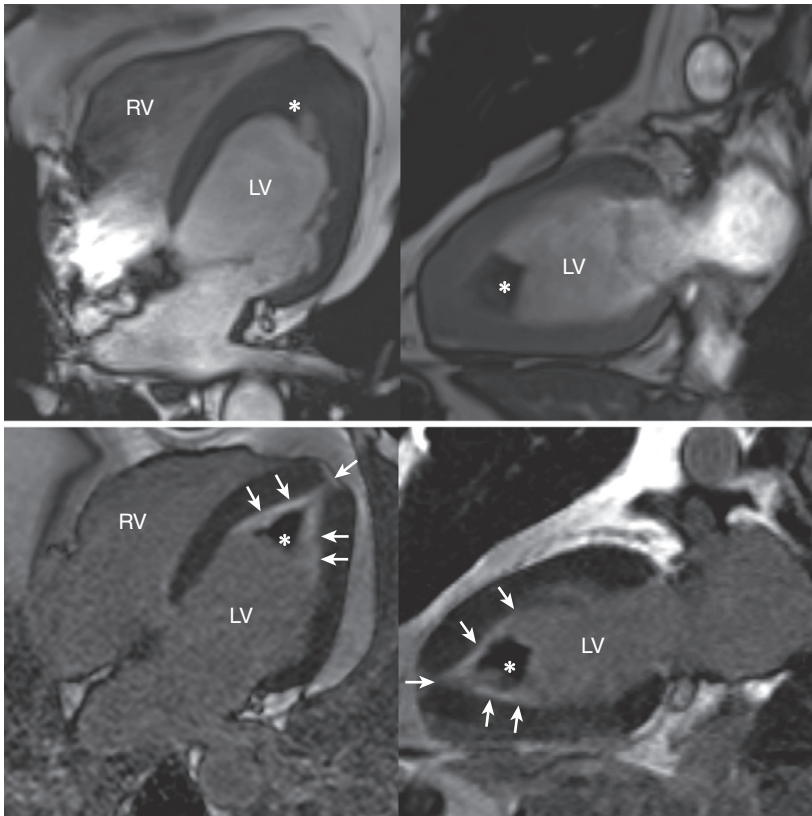


FIGURE 19.14 Loeffler's cardiomyopathy. **Top**, CMR in a 63-year-old man with fatigue, elevated eosinophil count, and echocardiogram suggestive of LV apical thrombus revealed normal LV and RV systolic function with obliteration of the LV apex on SSFP cine sequences in four-chamber and two-chamber projections (see Videos 19.9 and 19.10). **Bottom**, LGE imaging with phase-sensitive inversion recovery revealed subendocardial LGE at the LV apex (arrows) with overlying apical thrombus (asterisk). Collectively these findings are consistent with endomyocardial fibrosis (Loeffler's endocarditis). (Courtesy Aldo Schenone, MD, Brigham and Women's Hospital, Boston.)

Other Cardiomyopathies

Iron-overload cardiomyopathy is either inherited or acquired (see Chapter 52). In patients with transfusion-dependent thalassemia major, cardiac death as a result of myocardial iron toxicity occurs in 50% of patients. Global systolic LV function is usually preserved, especially in anemic thalassemic patients, until severe cardiac toxicity has developed, and thus provides little if any guidance to chelation therapy. Quantitative T2* was extensively validated and demonstrated an inverse exponential relationship with myocardial iron content. The use of T2* in guiding the use of iron-chelation therapy had led to a substantial reduction of mortality in patients with thalassemia major. In patients with reduced ventricular function, a T2* <20 msec (at 1.5T) is consistent with iron overload, whereas a myocardial T2* <10 msec indicates a high risk of clinical heart failure, despite normal LV function, within 1 year T2* imaging on a 3T scanner provides similar clinical guidance as 1.5T, although measurements have higher reproducibility at 1.5T for iron-overload cases.⁴⁵ On the other hand, recent data indicates that T1 has high concordance with T2* in characterizing myocardial iron; indeed using a cutoff value of 800 msec (at 1.5T) is more sensitive in detecting mild iron overload than T2*. Transient LV apical ballooning syndrome (or Takotsubo cardiomyopathy), precipitated by elevated catecholamines from severe emotional or physical stress, is characterized by a transient circumferential contractile dysfunction of the apex, which is in stark contrast to basal hyperkinesia. A variant of mid-LV akinesia sparing the apex has been reported affecting as many as 40% of patients. Myocardial edema by T2-weighted imaging and perfusion defects consistent with microvascular dysfunction, matching the segments with severe systolic dysfunction, are common. LGE imaging in most cases are negative

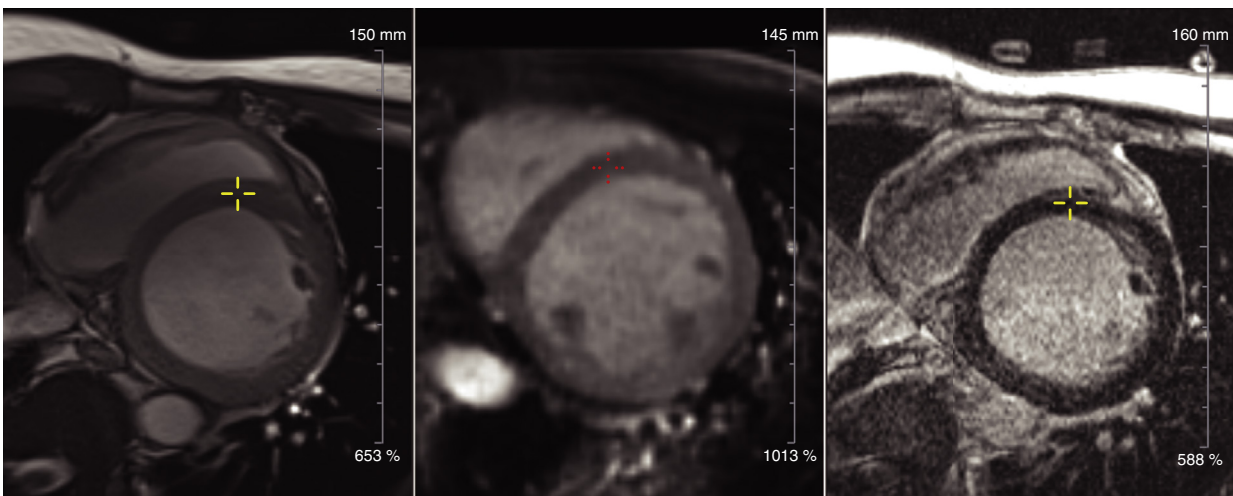


FIGURE 19.15 Idiopathic dilated cardiomyopathy. CMR diagnosis of nonischemic dilated cardiomyopathy relies on demonstration of LV dilation and systolic dysfunction (left, see also Video 19.11) and ruling out other causes of cardiomyopathy. In this case, there was absence of both stress perfusion defect (middle) and LGE (right) so that infarction and infiltration were ruled out. In approximately 30% of patients with idiopathic cardiomyopathy, there is a characteristic mid-wall striate of LGE.

or showing only a low-intensity diffuse enhancement (<5 SD above remote myocardium) in the dysfunctional segments. Indeed, significant LGE should raise the suspicion for an alternative diagnosis of an acute coronary event. A recent study of ultrasmall superparamagnetic iron-oxide enhanced CMR demonstrated that macrophage-mediated inflammation may last for several months and is associated with clinical heart failure in patients with Takotsubo cardiomyopathy.⁴⁶

At an investigational level, tissue mapping and feature-tracking strain analysis have expanding applications. CMR tissue mapping has remarkably high negative predictive value for clinically significant cardiac allograft rejection for obviation of routine invasive endomyocardial biopsy and capability of monitoring treatment.^{47,48} For patients with pulmonary hypertension, CMR feature tracking RV strain correlates well with invasive RV-pulmonary arterial uncoupling and RV end-diastolic stiffness.⁴⁹ In patients who received anthracycline chemotherapy, T1, T2, and ECV mapping appears to have higher sensitivity than global longitudinal strain in detecting subclinical cardiotoxicity and may help in dose titration.⁵⁰

Valvular Heart Disease (see Part VIII)

With capability to quantify cardiac volumes, valvular and great vessel flow hemodynamics, 3D angiography, and the lack of acoustic window limitation, CMR is complementary to echocardiography in quantifying valvular dysfunction and its associated cardiac consequences.

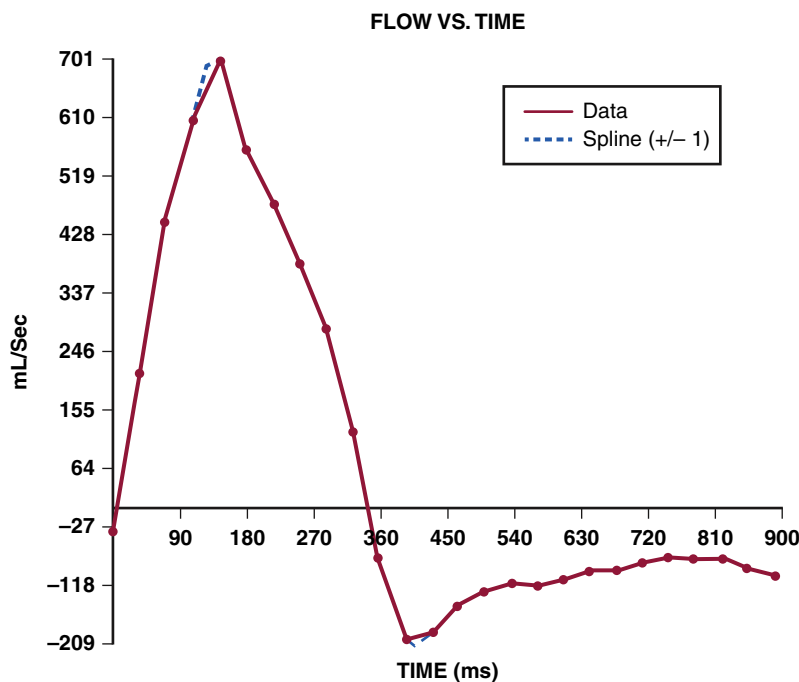
Aortic Stenosis

For aortic stenosis (see Chapter 72), aortic valve area, by planimetry or estimates from pressure gradients, is reliable and can be measured in most native aortic valves without severe calcifications.⁵¹ As myocardial consequences are the most common in severe valvular disease if not timely managed, some argue that CMR methods can better time intervention than an isolated assessment of valvular severity. Diffuse (patchy LGE) or replacement (endocardial) myocardial fibrosis often coexist in the pressure-loaded LV myocardium in patients with severe aortic stenosis. (see Figs. 72.6 and 72.7) In one study, presence of LGE scar, seen in 57% of the cohort, was associated with severe adverse LV remodeling, a doubling of mortality risk over 3.6 years.⁵² Another study observed that ECV fraction by CMR before transcatheter aortic valve replacement (TAVR) provided strong association with mortality adjusted to LV ejection fraction and LGE (see Fig. 72.8A).⁵³ Using CMR spectroscopy, it has been reported that a de-energized myocardial state already developed in most moderate grade aortic stenosis.⁵⁴ These studies in combination challenges the notion if an earlier CMR-guided TAVR intervention should be implemented to improve patient outcomes. In elderly patients, coexistence of amyloidosis was noted by CMR in 8% of patients manifesting a low-flow low-gradient pattern, and it has poor prognosis.⁵⁵ CMR is a useful tool in assessing patients before or after TAVR (see Chapter 74). Compared with transthoracic echocardiography, CMR is more accurate in sizing the aortic annulus before the procedure, which predicts the severity of aortic regurgitation after TAVR. It has also been shown to be more sensitive in detecting significant paravalvular aortic regurgitation after TAVR. Metallic artifacts from prosthetic aortic valve may limit CMR assessment of aortic valvular dysfunction.

Aortic Regurgitation

For aortic regurgitation (see Chapter 73), CMR phase contrast imaging quantifies regurgitant volume without the need for geometric assumption, thus has higher reproducibility than echocardiography and is more suitable for serial monitoring (Fig. 19.16 and Videos 19.12 through 19.18;

see also Fig. 73.6). A recent study of 232 patients with chronic aortic regurgitation, CMR and echocardiography were discordant by two or more grades in 41% of patients, the majority of whom were considered to have severe aortic regurgitation by echocardiography. At a 3-year follow-up, only N-terminal pro-BNP and severe aortic regurgitation by CMR were significant predictors for heart failure and death.⁵⁶ The ability of CMR to provide high quality imaging of structure and physiology of the great vessels may complement the assessment of valvular



B Slice position: SP H5.0 Venc adjustment -250 : 250

FIGURE 19.16 Bicuspid aortic valve with aortic regurgitation and ascending aortic aneurysm. **A**, CMR of a patient with bicuspid aortic valve with significant calcific degenerative changes. **B**, Severe aortic regurgitation (regurgitant volume 60 mL on velocity flow mapping). Serial imaging (Videos 19.12 and 19.13) revealed severe aortic regurgitation (regurgitant volume 60 mL on velocity flow mapping) (Video 19.14), moderate LV dilation, normal ejection fraction (58%), and ascending aortic aneurysm. He developed symptoms and underwent aneurysm repair and valve replacement with a bioprosthesis, which is well seated without regurgitation (Videos 19.15 and 19.16), with associated reverse remodeling with LV end-diastolic volume decreasing from 279 mL to 137 mL (Videos 19.17 and 19.18).

dysfunction. 4D flow imaging can identify vortical blood flow pattern in the pulmonary artery and estimate mean pulmonary arterial pressures noninvasively. In addition, in patients with bicuspid aortic valve, visualization of vascular “vector” flow can determine vascular wall shear stress and systolic flow eccentricity, potentially predicting development of bicuspid aortic valvular aortopathy.

Mitral Regurgitation

Echocardiography is highly available and clinically adapted in assessment of mitral regurgitation as the principal technique, but it has significant interpretive variability due to characteristics of the regurgitant jet and requires major assumptions in its quantitative methods. Similar to echocardiography, CMR can visualize mitral leaflet and regurgitant jet morphology in multiple views (see [Chapters 16 and 76](#)). However, CMR can quantify mitral regurgitation without major assumption, as the difference between LV stroke volume and forward stroke volume using cine SSFP and phase-contrast imaging, respectively. CMR also provides highly accurate and reproducible assessment of LV and left atrial function and volumes. Cine CMR and phase-contrast are most often acquired in 2D currently; thus some efforts and experience are needed to ensure precise placement of imaging scan planes and elimination of base phase offset errors.⁵⁷ Significant discordance had been reported between echocardiography and CMR, where an agreement of severe regurgitant status achieved in less than 70% was reported in most studies. When echocardiographic flow convergence and Doppler-based methods or 3D echocardiography were used to quantify regurgitant volume, the agreement with CMR slightly increased. In general, 2D echocardiography diagnoses severe mitral regurgitation substantially more

frequently and reports higher regurgitant volume than CMR. CMR has the advantage of accounting for flows in the entire cardiac cycle rather than reliance on a single point in time by some echocardiographic Doppler methods. CMR may provide more robust prediction of subsequent development of an indication for mitral valve surgery or heart failure mortality than echocardiography.⁵⁸ In patients who had severe mitral regurgitation by echocardiography and underwent mitral valve surgery, CMR regurgitant volume demonstrated stronger correlation to postsurgery reversal of LV remodeling than echocardiography. Adding tissue characterization to CMR scanning of mitral regurgitation may help with patient risk assessment. A single-center study demonstrated that LGE evidence of fibrosis was prevalent in patients with mitral regurgitation secondary to leaflet prolapse, and it was associated with ventricular arrhythmic events or sudden death.⁵⁹ In patients with CAD, LGE infarct size and ischemic mitral regurgitation severity by CMR were additive in patient risk assessment⁶⁰ ([Fig. 19.17](#) and [Videos 19.19 to 19.23](#)).

Tricuspid Regurgitation

CMR quantifies tricuspid regurgitant volume by the difference of RV stroke volume and pulmonary arterial forward volume. In small studies, moderate to high agreement was reported between echocardiography and CMR grading of tricuspid regurgitation severity.⁶¹

Pericardial Disease (see [Chapter 86](#))

Echocardiography in most cases should be performed first-line as it offers a rapid assessment of the pericardial structures and physiologic significance from pericardial constriction or cardiac tamponade, but a

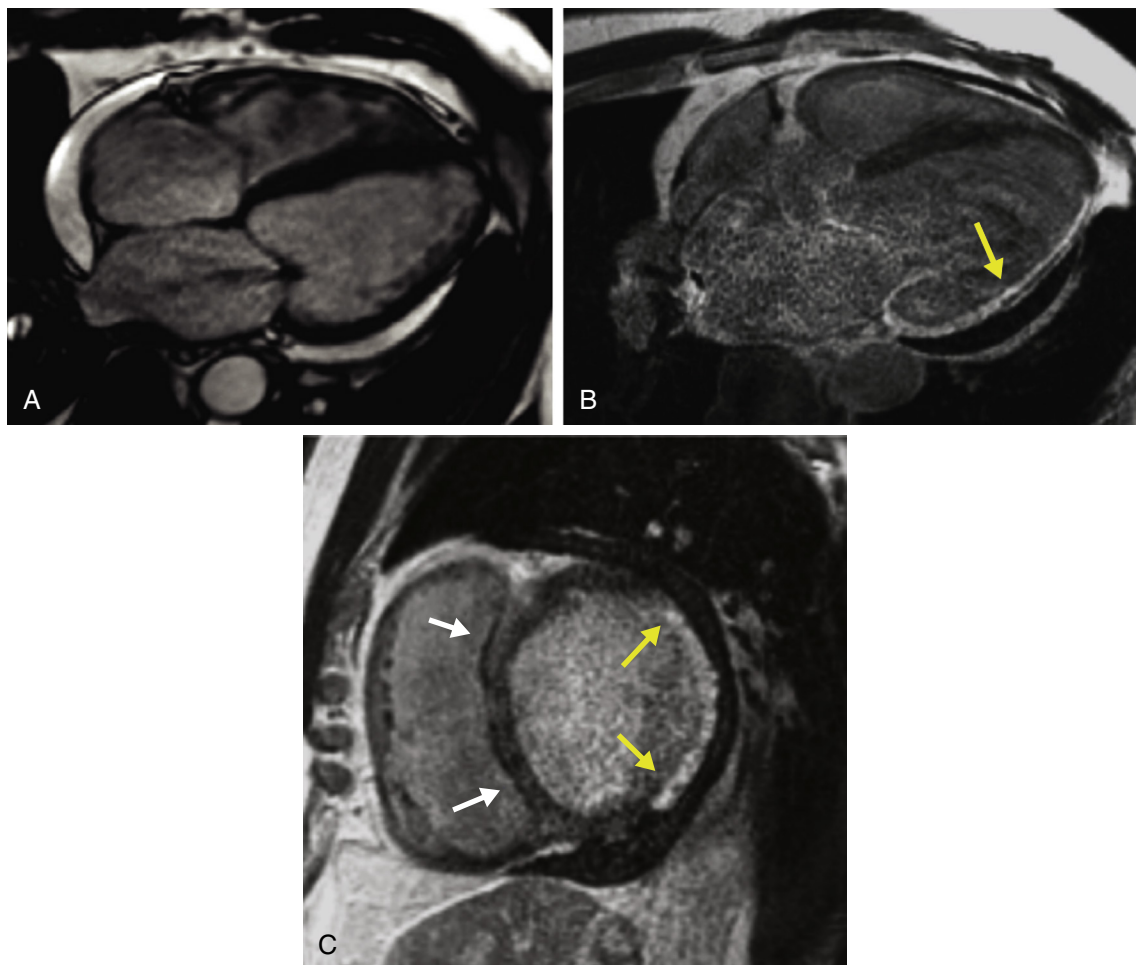


FIGURE 19.17 Ischemic mitral regurgitation. **A**, CMR in a 70-year-old man with new-onset heart failure in the setting of ischemic cardiomyopathy revealed severe biventricular dysfunction, akinesia of the lateral wall, and severe mitral and tricuspid regurgitation ([Videos 19.19 and 19.20](#)). Volumetric analysis confirmed marked LV dilation and dysfunction (LVEDV 185 mL and ejection fraction 21%) ([Video 19.21](#)). Flow velocity mapping across the aortic valve showed a stroke volume of 20 mL, with a regurgitant fraction of 48%, confirming severe mitral regurgitation ([Videos 19.22 and 19.23](#)). **B** and **C**, LGE images showed a lateral wall transmural myocardial infarction (*yellow arrows*) together with tethering of the posterior mitral leaflet. In addition, midwall septal fibrosis (*white arrows*) suggested mixed ischemic and nonischemic cardiomyopathy.

CMR offers a comprehensive assessment complementary to echocardiography in hemodynamically stable patients. A typical CMR protocol for pericardial diseases includes cine SSFP (pericardial structures), T1- and T2-weighted black-blood FSE (structures and T2-STIR imaging for edema), and LGE imaging (pericardial inflammation). In patients with suspected constriction, real-time cine SSFP (with or without Valsalva) may detect respirophasic septal shift due to ventricular interdependence. First-pass perfusion and contrast T1-weighted imaging may determine vascularity of a pericardial mass (e.g., differentiate tumor versus thrombus). Myocardial tagging (dark lines or grids) may identify regional concordance from pericardial adhesions. Pericardial thickness can be shown on either black-blood FSE or cine imaging, where up to 2 mm is considered normal; however, minimal but diffuse increased thickness is observed in 20% of patients with significant pericardial constriction. Pericardial LGE after the administration of GBCA indicates active pericardial inflammation and has been shown to complement C-reactive protein levels in diagnosing active pericarditis and predicting reversibility of pericardial inflammation and even constrictive physiology in response to anti-inflammatory medical therapies (Fig. 19.18 and Videos 19.24 to 19.26). A recent study demonstrated quantitative pericardial LGE extent could predict the likelihood of clinical recurrence of pericarditis, incremental to clinical and inflammatory biomarkers.⁶² Simple pericardial cysts usually have thin smooth walls without internal septa and their transudative contents appear homogeneous dark on T1-weighted images and bright on T2-weighted images, with no enhancement after contrast. Proteinaceous cysts are bright on T1 but dark on T2-weighted images. Exudative pericardial fluid has medium intensity on T1-weight images. Hemorrhagic effusion is bright on both T1- and T2-weighted images but darkens as hemosiderin deposition occurs as it develops into a hematoma with variable intensity. All of the previously mentioned interpretations of signal intensities on T1- and T2-weighted images need to consider the effects of through-plane flow in black-blood imaging with time-of-flight

effects. Pericardial metastases are far more common (from lung, breast, and lymphomas) than primary pericardial tumors. Malignant invasion of the pericardium often shows focal obliteration of the pericardial line and a pericardial effusion. Most neoplasms appear dark or gray on noncontrast T1-weighted images except metastatic melanoma owing to its paramagnetic metals bound by melanin. Similar to CMR, computed tomography (CT) also accurately assesses the pericardial and cardiac structures, but it offers less tissue characterization or physiologic information than CMR.

APPLICATIONS IN CARDIAC ELECTROPHYSIOLOGY

CMR is helpful in planning electrophysiologic procedures given its ability to identify potential sites of ablation or scar and provide a 3D volume mapping of the atria or ventricles. For patients with paroxysmal atrial fibrillation (AF) undergoing pulmonary venous isolation (see Chapters 64 and 66), left atrial emptying function and LGE evidence of fibrosis are strong markers of AF recurrence. For those with postablation AF recurrence, atrial LGE from prior ablation can improve the success rate of a repeat pulmonary venous isolation by localizing ablation gaps and reduce procedural duration and radiofrequency application time. Although still early in development, CMR offers promise in characterizing mechanical dyssynchrony in heart failure patients and information relevant to placement of the LV pacing lead, such as coronary venous anatomy and LV scan location.

Risk Stratifying Patients at Risk of Sudden Death

CMR contributes to assessment of patients at risk of sudden death (SD) by quantitation of LV ejection fraction, RV pathology, detection of myocardial scar using LGE, anomalous coronary arteries, and less commonly T2* mapping for iron overload.³⁸ LV structures and LGE pattern in combination differentiate most patients in this setting as ischemic, non-ischemic, and infiltrative, which provides clinical guidance and patient risk profile (see Chapter 70). In SD survivors, LGE identified unexpected myocardial scar and a potential arrhythmic substrate in more than 70% of patients. For patients with CAD, multiple single-center studies have

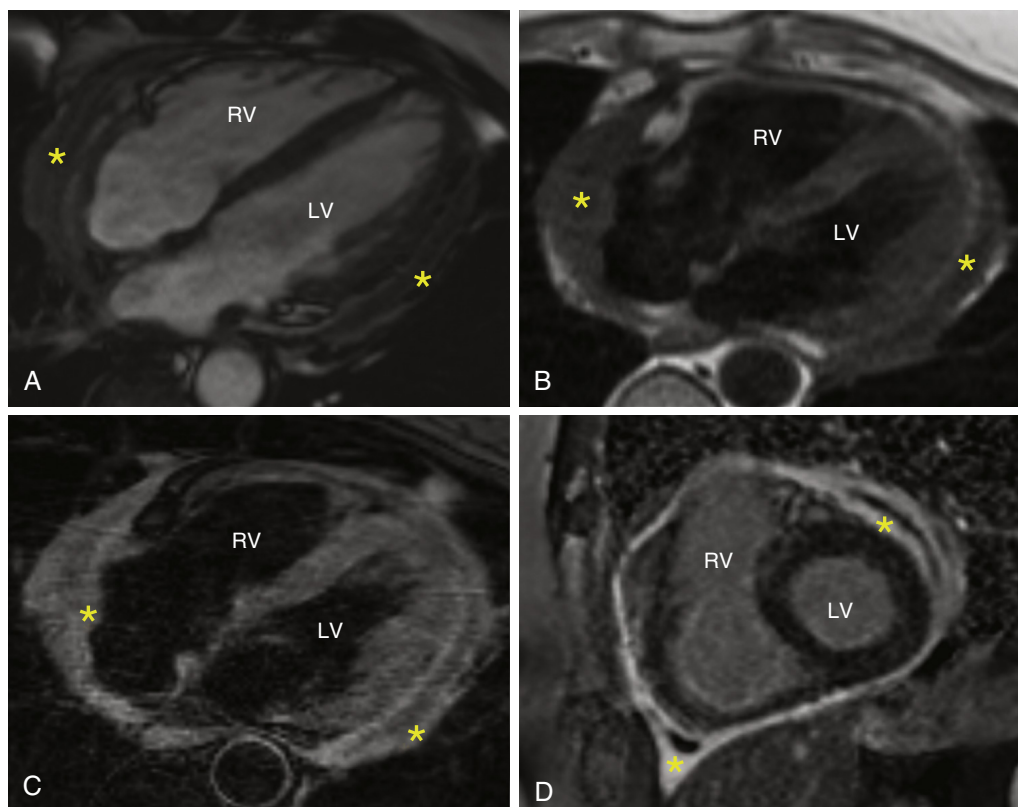


FIGURE 19.18 Constrictive pericarditis. CMR in a 66-year-old woman with recent acute pericarditis and worsening pain and dyspnea despite anti-inflammatory therapy revealing normal LV and RV systolic function (Video 19.24). Both SSFP cine (A) and T1-weighted fat suppressed (B) sequences revealed diffuse pericardial thickening (asterisks). C, Both pericardial layers exhibited diffuse hyperintensity on T2-weighted images consistent with pericardial edema (asterisks). D, The pericardium enhanced on first-pass perfusion images (Video 19.25) and demonstrated severe concentric LGE (asterisks) signaling pericardial inflammation. There was no respirophasic shift of the interventricular septum on real-time cine acquisition with Valsalva (Video 19.26) to support a diagnosis of transient constriction. With evidence of acute pericarditis without constriction, the patient was treated with prednisone in addition to nonsteroidal anti-inflammatory agents and colchicine with eventual symptomatic improvement. (Courtesy Aldo Schenone, MD, Brigham and Women's Hospital, Boston, MA.)

reported LGE size as robust risk marker for SD independent of left ventricular ejection fraction (LVEF). Larger than 5% of LV mass has been reported to be a risk marker in both ischemic and nonischemic cardiomyopathies. Scar texture and scar heterogeneity might carry additional information. A multicenter long-term follow-up outcome study of heart failure patients with implanted ICD equipped with cardiac resynchronization therapy showed that a lack of LGE fibrosis was protective but greater presence of border zone channel heterogeneity identified life-threatening ventricular arrhythmias incrementally, thus raising the possibility for better triage of ICD candidates.⁶³ For patients with nonischemic cardiomyopathy, a mid-wall septal LGE pattern has a noted in many patients with dilated cardiomyopathy and its size has been reported to be associated with inducibility of ventricular arrhythmias and SDs. LV LGE in patients with systemic sarcoidosis has a high risk of SD. More research is needed to define how the LGE extent can improve the current practice guidelines specifically toward ICD therapy.

ADULT CONGENITAL HEART DISEASE

CMR can complement other imaging for adult congenital heart disease (see [Chapter 82](#)) based on several factors: lack of radiation exposure to young patients, 3D tomographic imaging of thoracic structures and anatomy (compared with the more limited echocardiographic windows with body growth), and correlation of complex anatomy with blood flow and physiology.

Atrial and Ventricular Septal Defects

CMR offers a less invasive alternative to transesophageal echocardiography and even diagnostic catheterization for patients presenting with right-sided volume overload from a suspected left-to-right shunt. A CMR study can detect the presence of an atrial septal defect (ASD), assess suitability for transcatheter ASD closure ([Fig. 19.19](#) and [Video 19.27](#)), quantify right heart size and function by cine SSFP, determine pulmonary-to-systemic shunt ratio (Qp/Qs) using velocity-encoded phase-contrast, and identify any coexisting anomalous pulmonary venous return using 3D contrast-enhanced MRA. Phase-contrast imaging positioned in a plane parallel to the atrial septum and set at a low velocity range (100 cm/sec) can visualize the ASD *en face* with good correlation with defect size measured invasively. Phase-contrast imaging of the tricuspid regurgitation can estimate the pulmonary arterial systolic pressure. Because most closure devices are MRI compatible, CMR can be used to assess for residual shunt and proper device deployment. Patients with a ventricular septal defect (VSD) can be assessed using similar CMR techniques. In addition, LGE imaging may help to determine if a VSD has developed as a complication from an MI.

Anomalous Pulmonary Venous Connection

Using a large field of view, 3D MRA can capture abnormal intrathoracic structures and vascular dynamics in anomalous pulmonary venous return ([Fig. 19.20](#) and [Video 19.28](#)). Near-isotropic in-plane resolution can be achieved allowing reformatting in any plane to

detect anomalous venous structures as small as 1 mm. The magnitude of any left-to-right shunt can be assessed by either direct blood flow measurement in the anomalous pulmonary vein or Qp/Qs ratio described previously, which is in general more accurate than invasive oximetry measurements due to the errors from mixed venous return in the right atrium.

Coarctation of the Aorta

Gadolinium-enhanced 3D MRA is sufficient in defining the site of aortic narrowing in most cases of aortic coarctation. Cine SSFP in a long-axis “candy-cane” view can further delineate the aortic anatomy, the degree of obstruction, and aortic valvular dysfunction. Cine SSFP is the gold standard for LV size, LV function, and myocardial mass. Black-blood FSE is useful to evaluate the entire aorta because it is less affected by metallic artifacts from implanted endovascular stent than gradient-echo techniques. Phase-contrast imaging can characterize the descending-to-ascending aorta flow ratio and estimate pressure gradient across the coarctation and collaterals formation ([Fig. 19.21](#) and [Video 19.29](#)).

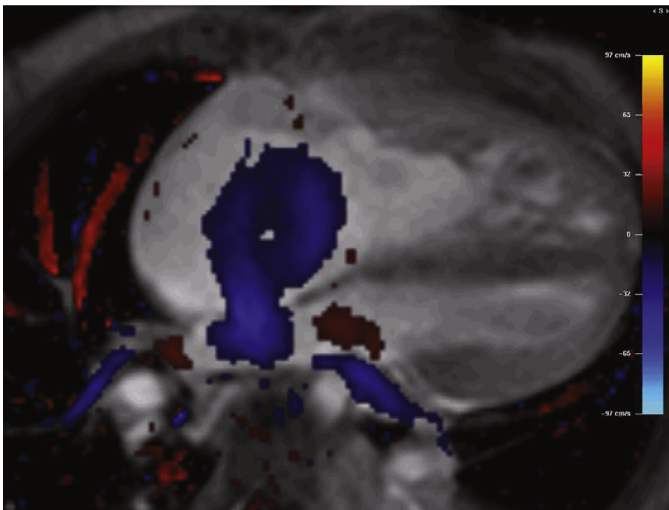


FIGURE 19.19 Secundum atrial septal defect. Color-coded phase contrast imaging demonstrated large left atrial to right atrial flow with resultant right atrial and ventricular dilation. See [Video 19.27](#). (Courtesy Drs. Andrew J. Powell and Rahul H. Rathod, Boston Children’s Hospital.)

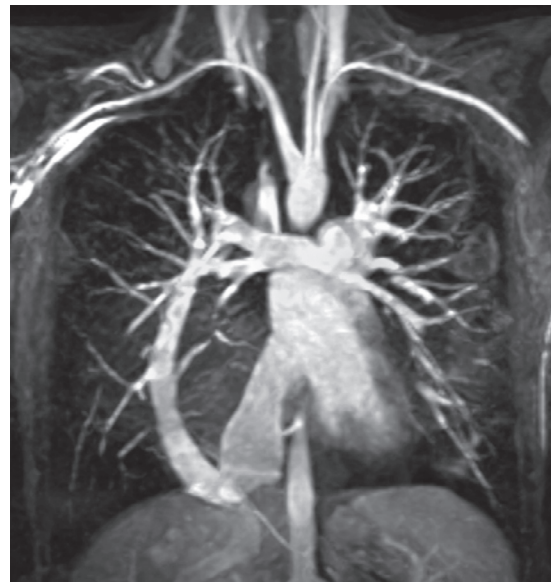


FIGURE 19.20 Scimitar syndrome. Gadolinium-enhanced 3D MRA (oblique coronal subvolume maximal intensity projection) in an adult with scimitar syndrome (see [Video 19.28](#)). (Courtesy Drs. Andrew J. Powell and Rahul H. Rathod, Boston Children’s Hospital.)



FIGURE 19.21 Aortic coarctation. Volume rendered gadolinium-enhanced 3D MRA (see [Video 19.29](#)) in a patient with aortic coarctation reveals several tortuous collateral vessels and dilated internal mammary arteries. (Courtesy Drs. Andrew J. Powell, MD, and Rahul H. Rathod, MD, Boston Children’s Hospital.)

**Conotruncal Anomalies**

Tetralogy of Fallot (TOF) is an increasingly common referral. In patients being planned for surgical repair, key elements provided by CMR include depiction of all sources of pulmonary blood flow (including pulmonary arterial, aortopulmonary collateral, and ductus-arterial sources) in presence of RV outflow obstruction, quantitation of the severity of infundibular or pulmonary stenosis, assessment of RV function, and ruling out a coexisting anomalous coronary artery. In patients who have undergone surgery for TOF, CMR provides relevant assessment for any RV outflow aneurysm, pulmonary regurgitation fraction (patients who underwent patching of the pulmonary valve with post-operative pulmonary regurgitation), biventricular size and function,

and any residual shunt. LGE imaging has been proposed for detection of myocardial fibrosis, which is associated with ventricular dysfunction, exercise intolerance, and arrhythmias. The principle physiologic abnormality in D-loop transposition of the great arteries (TGA, D-loop being the most common type of TGA) is profound hypoxemia due to ventriculoarterial discordant connection where systemic venous blood goes to the aortic and oxygenated pulmonary venous blood returns to the lung. Survival is dependent on systemic-pulmonary circulatory mixing via a ductus arteriosus, an ASD, or a VSD. An arterial switch operation is now the most common corrective surgery, but many adult patients have undergone an atrial switch procedure. CMR is useful in monitoring these patients after surgical correction by serially assessing ventricular size and function, flow across the postoperative LV and RV outflow tracts, and aortopulmonary collaterals. Systemic RV LGE is strongly associated with adverse clinical outcome especially arrhythmia in transposition of the great arteries; thus LGE CMR should be incorporated in risk stratification of these patients.

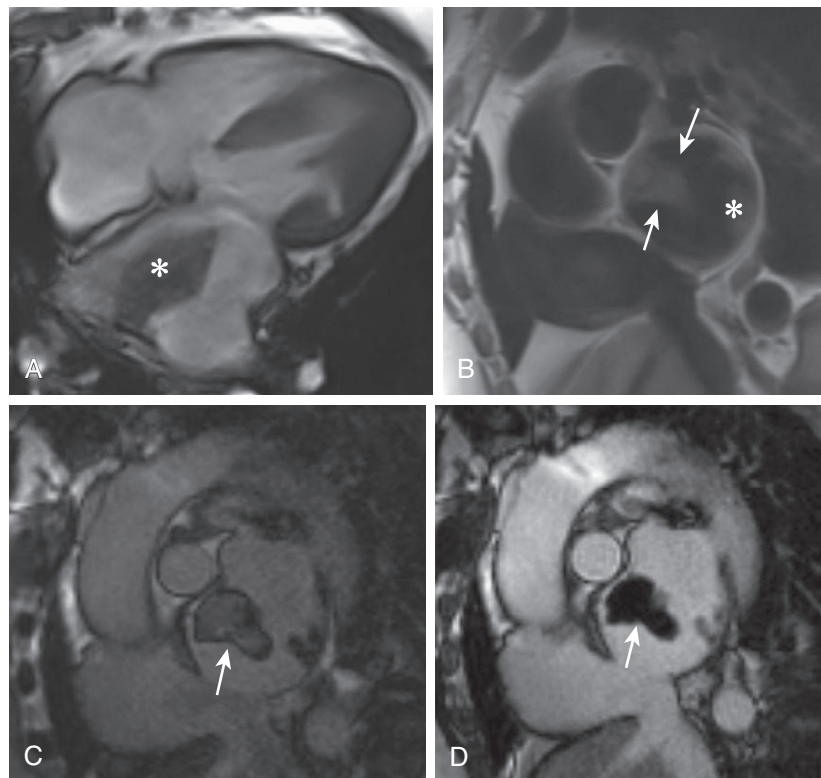


FIGURE 19.22 Cardiac thrombus. CMR in a 66-year-old woman with factor V Leiden mutation and antiphospholipid syndrome and finding of a mass on echocardiography. **(A)** Steady-state free precession image, four-chamber view demonstrates an isointense mass in the left atrium posterior wall (*asterisk*). **(B)** T1-weighted black-blood image, short-axis view demonstrates an isointense mass attached to the left atrial wall (*arrows*). There is another small mass in the posterior wall of the atrium (*asterisk*), which suggests presence of multiple thrombi. **(C)** On LGE image, short-axis view, the mass appears to be heterogeneously hyperintense, while **(D)** on LGE, long inversion time (T1) image (T1 = 600 ms), short-axis view, the mass was nulled completely suggesting lack of enhancement. These findings are consistent with multiple intracardiac thrombi.

CARDIAC THROMBUS AND MASS

The differential diagnoses of an intracardiac mass includes a thrombus, tumor, or vegetation (see [Chapter 98](#)). LGE imaging can detect thrombus at a higher sensitivity than echocardiography by depicting high contrast between the dark thrombus and its adjacent structures and by imaging in 3D. Mural thrombus does not enhance on first-pass perfusion and often has a characteristic “etched” appearance on LGE imaging, thus providing higher diagnostic specificity than anatomical information alone. Multiple pulse sequences can be used to detect vascularity of tumor after contrast injection and allow differentiation from thrombus ([Fig. 19.22](#)). A pattern of hyperintensity/isointensity (compared with normal myocardium) with short TI and hypointensity with long TI was very frequent in thrombi (94%), rare in tumors (2%), and the highest accuracy (95%) for the differentiation of both entities. Common benign cardiac tumors include atrial myxoma, rhabdomyoma, fibroma, and endocardial fibroelastoma. Atrial myxomas are often seen as a round or multilobar mass in the left atrium (75%), right atrium (20%), and ventricles or mixed chambers (5%) ([Fig. 19.23](#) and [Videos 19.30](#) and [19.31](#)). They typically have inhomogeneous brightness in the center on cine SSFP imaging due to gelatinous contents and may have a pedunculated attachment to the fossa ovalis. Metastatic cardiac malignancy is much more common than primary cardiac malignancy; malignant lesions include cardiac involvement from direct invasion (lung and breast), lymphatic spread (lymphomas and melanomas), and hematogenous spread (renal cell carcinoma). Primary cardiac malignancies occur more often in children or young adults. They include angiosarcoma, fibrosarcoma, rhabdomyosarcoma, and liposarcoma. CMR in a multicenter trial correctly diagnosed 97% of these cases although a differential diagnosis was necessary in 42%.

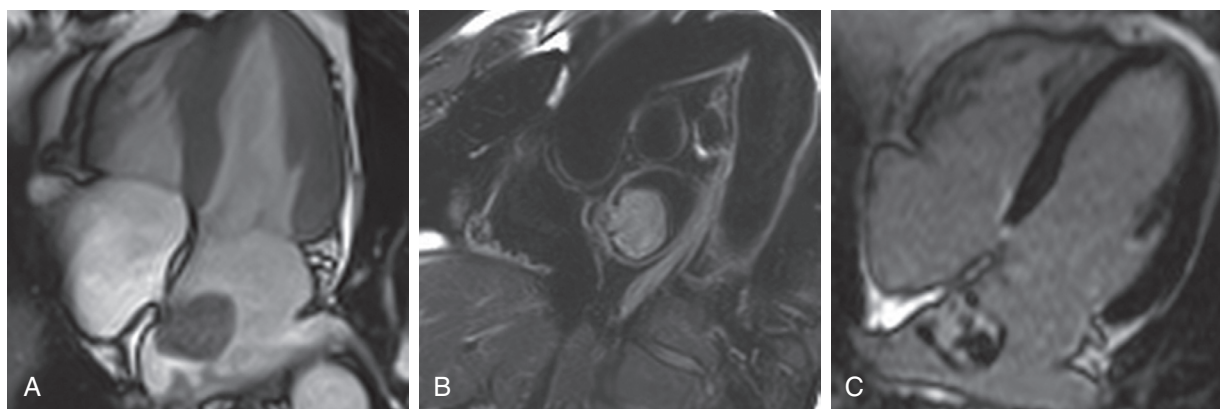


FIGURE 19.23 Cardiac myxoma. **A**, CMR in a 24-year-old woman with suspicion of a left atrial mass on echocardiography revealed evidence of a left atrial myxoma adherent to the interatrial septum on cine functional four-chamber and basal short-axis (see [Videos 19.30](#) and [19.31](#)). **B**, Tissue characterization revealed hyperintense signal on T2-weighted sequence suggestive of tissue edema. **C**, There was heterogeneous signal intensity on LGE imaging. Subsequent histopathology confirmed the diagnosis after surgical resection resulting in symptom resolution. (Courtesy Naeem Merchant, MD, and Bobak Heydari, MD, MPH. Stephenson Cardiac Imaging Center, University of Calgary, Calgary, Canada.)

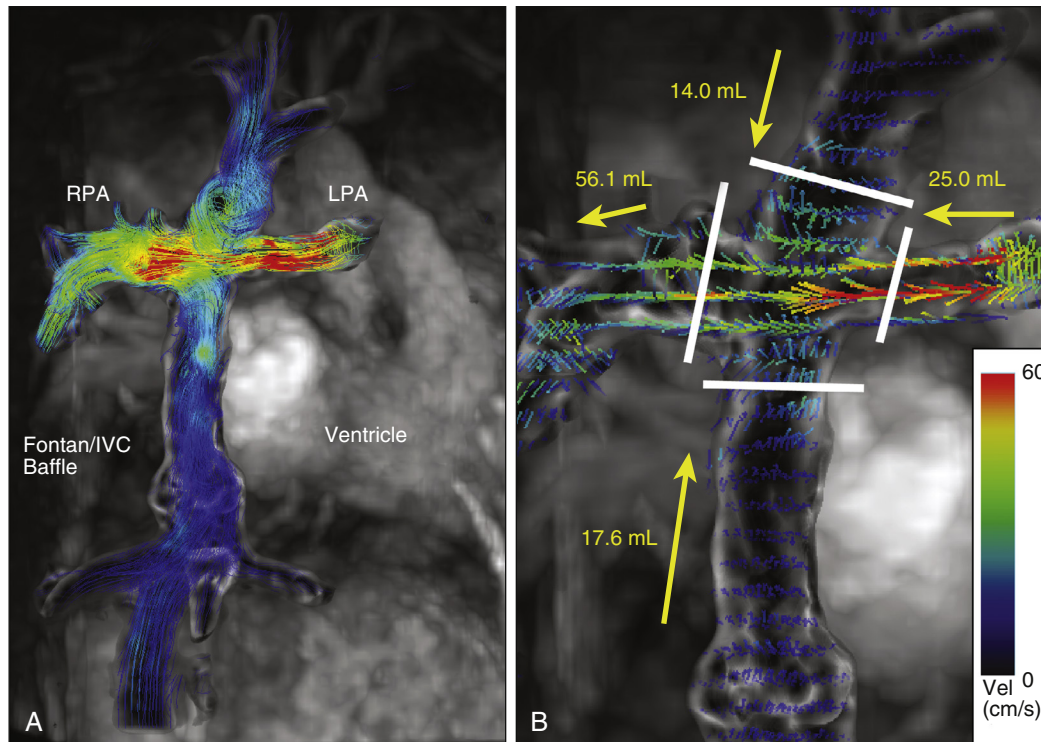


FIGURE 19.24 Four-dimensional flow imaging in a 12-year-old girl with congenital heart disease, including right dominant atrioventricular defect and previous Fontan operation. Routine clinical MRA showed a hypoplastic left pulmonary artery (LPA) without stenosis and a moderately dilated right pulmonary artery (RPA). **A**, 4D flow visualization using time-resolved pathlines and vector representations demonstrated the unique case that all caval flow was directed to the RPA, and there was complete retrograde flow in the LPA due to an extensive aortopulmonary collateral burden to the left lung. These observations were confirmed by comprehensive flow quantification in the Fontan connection: 2D planes were retrospectively placed in the 4D flow MRI to quantify flow in the superior vena cava and inferior vena cava baffle (SVC, IVC), as well as the RPA and LPA. **B**, For flow quantification accuracy assurance, 4D flow MRI could be used to check flow conservation: Using the net flow values depicted in **(B)** net flows ($[LPA] + [SVC] + [IVC]$) = 56.6 mL/cycle, which was equal to RPA net flow. **A**, Depicts 3D streamlines in mid diastole released from the Fontan anastomoses. **B**, A zoomed-in view depicts vectorized representation of flow velocities, with large yellow arrows indicating the primary direction of flow. White lines indicate retrospective placement of 2D orthogonal analysis planes for 4D flow quantification, with associated numbers representing net flow through each plane (mL/cycle). (See also Video 19.32.) (Courtesy Liliana Ma, Cynthia Rigby, Matthew Cornicelli, and Michael Markl, Departments of Medical Imaging and Radiology, Northwestern University.)

NOVEL CMR IMAGING TECHNIQUES AND FUTURE PERSPECTIVES

Technologic advance of CMR in the next years will likely focus on improving the study throughput, protocol consistency, and patient tolerability. Compressed sensing was a signal processing breakthrough in 2004, which discovered that digital images can be reconstructed with data sample rates even lower than Nyquist's Law because information content of CMR images is compressible. Compressed sensing has shown promise in substantially improving the efficiency of CMR cine, perfusion, 4D flow (Fig. 19.24 and Video 19.32), and coronary MRA.⁶⁴ It allows increasing clinical use of high quality real-time imaging of cardiac function without any need for cardiac gating or breath holding or acquisition of the whole-heart cine at high resolution in a single breath-hold. Pulse sequences that acquire a 3D dataset achieve a whole cardiac coverage at higher consistency than 2D and have shown clinical promise in perfusion imaging and LGE imaging. Automated motion correction reduces blurring from cardiac motions and has become standard in many pulse sequences because it not only improves qualitative visual displays but also facilitates quantitative measurements. Artificial intelligence-guided cardiac localization and scanning algorithms have been developed and are now commercially available to increase scanning consistency and may reduce scan time by 40% to 60%. Although MRI technology in general moves in the direction of higher field strength owing to the benefits of improved signal-to-noise ratio, low field CMR (field strength <1.0T) is a focus of active investigations and is promising in enhancing the clinical adaptation of CMR. Compared with current routine of 1.5 or 3T, low field CMR has potential benefits unique to cardiac patients: lower scanner and site construction cost, fewer artifacts and easier

performance, and less heat deposition and thus safer for patients with metallic devices.⁶⁵ It appears that the loss in signal-to-noise ratio can be gained back by the use of SSFP methods or appropriate revision of pulse sequence settings (e.g., increasing flip angle) without significant risk of tissue heating.⁶⁶

REFERENCES

Principles of Magnetic Resonance Imaging

- Nazarian S, Hansford R, Rahsepar AA, et al. Safety of magnetic resonance imaging in patients with cardiac devices. *N Engl J Med*. 2017;377:2555–2564.

Coronary Artery Disease

- Foley JRJ, Kidambi A, Biglunds JD, et al. A comparison of cardiovascular magnetic resonance and single photon emission computed tomography (SPECT) perfusion imaging in left main stem or equivalent coronary artery disease: a CE-MARC substudy. *J Cardiovasc Magn Reson*. 2017;19:84.
- Rijlaarsdam-Hermens D, Lo-Kioeng-Shioe M, van Dornburg RT, et al. Stress-only adenosine CMR improves diagnostic yield in stable symptomatic patients with coronary artery calcium. *JACC Cardiovasc Imaging*. 2020;13:1152–1160.
- Vincenti G, Masci PG, Monney P, et al. Stress perfusion CMR in patients with known and suspected CAD: prognostic value and optimal ischemic threshold for revascularization. *JACC Cardiovasc Imaging*. 2017;10:526–537.
- Kwong RY, Ge Y, Steel K, et al. Cardiac magnetic resonance stress perfusion imaging for evaluation of patients with chest pain. *J Am Coll Cardiol*. 2019;74:1741–1755.
- Ge Y, Pandya A, Steel K, et al. Cost-effectiveness analysis of stress cardiovascular magnetic resonance imaging for stable chest pain syndromes. *JACC Cardiovasc Imaging*. 2020;13:1505–1517.
- Biglunds JD, Ibraheem M, Magee DR, et al. Quantitative myocardial perfusion imaging versus visual analysis in diagnosing myocardial ischemia: a CE-MARC substudy. *JACC Cardiovasc Imaging*. 2018;11:711–718.
- Knott KD, Seraphim A, Augusto JB, et al. The prognostic significance of quantitative myocardial perfusion: an artificial intelligence based approach using perfusion mapping. *Circulation*. 2020;141:1282–1291.
- Nagel E, Greenwood JP, McCann GP, et al. Magnetic resonance perfusion or fractional flow reserve in coronary disease. *N Engl J Med*. 2019;380:2418–2428.
- Le TT, Bryant JA, Ting AE, et al. Assessing exercise cardiac reserve using real-time cardiovascular magnetic resonance. *J Cardiovasc Magn Reson*. 2017;19:7.
- Kim HW, Rehwald WG, Jenista ER, et al. Dark-blood delayed enhancement cardiac magnetic resonance of myocardial infarction. *JACC Cardiovasc Imaging*. 2018;11:1758–1769.
- Symons R, Pontone G, Schwitler J, et al. Long-term incremental prognostic value of cardiovascular magnetic resonance after ST-segment elevation myocardial infarction: a study of the collaborative registry on CMR in STEMI. *JACC Cardiovasc Imaging*. 2018;11:813–825.



13. Ibanez B, Aletras AH, Arai AE, et al. Cardiac MRI endpoints in myocardial infarction experimental and clinical trials: JACC scientific expert panel. *J Am Coll Cardiol*. 2019;74:238–256.
14. Everaars H, van der Hoeven NW, Janssens GN, et al. Cardiac magnetic resonance for evaluating nonculprit lesions after myocardial infarction: comparison with fractional flow reserve. *JACC Cardiovasc Imaging*. 2020;13:715–728.
15. Smulders MW, Kietselaer B, Wildberger JE, et al. Initial imaging-guided strategy versus routine care in patients with non-STsegment elevation myocardial infarction. *J Am Coll Cardiol*. 2019;74:2466–2477.
16. Dastidar AG, Baritussio A, De Garate E, et al. Prognostic role of CMR and conventional risk factors in myocardial infarction with nonobstructed coronary arteries. *JACC Cardiovasc Imaging*. 2019;12:1973–1982.
17. Lintings PF, Nivet H, Clement-Guinaudeau S, et al. High-resolution late gadolinium enhancement magnetic resonance for the diagnosis of myocardial infarction with nonobstructed coronary arteries. *JACC Cardiovasc Imaging*. 2020;13:1135–1148.

Cardiomyopathies

18. Vita T, Grani C, Abbasi SA, et al. Comparing CMR mapping methods and myocardial patterns toward heart failure outcomes in nonischemic dilated cardiomyopathy. *JACC Cardiovasc Imaging*. 2019;12:1659–1669.
19. Charron P, Elliott PM, Gimeno JR, et al. The Cardiomyopathy Registry of the EURObservational Programme of the European Society of Cardiology: baseline data and contemporary management of adult patients with cardiomyopathies. *Eur Heart J*. 2018;39:1784–1793.
20. Di Marco A, Anguera I, Schmitt M, et al. Late gadolinium enhancement and the risk for ventricular arrhythmias or sudden death in dilated cardiomyopathy: systematic review and meta-analysis. *JACC Heart Fail*. 2017;5:28–38.
21. Hindieh W, Weissler-Smir A, Hammer H, et al. Discrepant measurements of maximal left ventricular wall thickness between cardiac magnetic resonance imaging and echocardiography in patients with hypertrophic cardiomyopathy. *Circ Cardiovasc Imaging*. 2017;10:e006309.
22. Mentias A, Raesi-Giglou P, Smedira NG, et al. Late gadolinium enhancement in patients with hypertrophic cardiomyopathy and preserved systolic function. *J Am Coll Cardiol*. 2018;72:857–870.
23. Sivalokanathan S, Zghaib T, Greenland GV, et al. Hypertrophic cardiomyopathy patients with paroxysmal atrial fibrillation have a high burden of left atrial fibrosis by cardiac magnetic resonance imaging. *JACC Clin Electrophysiol*. 2019;5:364–375.
24. Ariga R, Tunnicliffe EM, Manohar SG, et al. Identification of myocardial disarray in patients with hypertrophic cardiomyopathy and ventricular arrhythmias. *J Am Coll Cardiol*. 2019;73:2493–2502.
25. Neubauer S, Kolm P, Ho CY, et al. Distinct subgroups in hypertrophic cardiomyopathy in the NHLBI HCM registry. *J Am Coll Cardiol*. 2019;74:2333–2345.
26. Marstrand P, Han L, Day SM, et al. Hypertrophic cardiomyopathy with left ventricular systolic dysfunction: insights from the SHARe registry. *Circulation*. 2020;141:1371–1383.
27. Aquaro GD, De Luca A, Cappellotto C, et al. Prognostic value of magnetic resonance phenotype in patients with arrhythmogenic right ventricular cardiomyopathy. *J Am Coll Cardiol*. 2020;75:2753–2765.
28. Kotanidis CP, Bazmpani MA, Haidich AB, et al. Diagnostic accuracy of cardiovascular magnetic resonance in acute myocarditis: a systematic review and meta-analysis. *JACC Cardiovasc Imaging*. 2018;11:1583–1590.
29. Oka E, Iwasaki YK, Maru Y, et al. Prevalence and significance of an early repolarization electrocardiographic pattern and its mechanistic insight based on cardiac magnetic resonance imaging in patients with acute myocarditis. *Circ Arrhythm Electrophysiol*. 2019;12:e006969.
30. von Knobelsdorff-Brenkenhoff F, Schuler J, Doganuzel S, et al. Detection and monitoring of acute myocarditis applying quantitative cardiovascular magnetic resonance. *Circ Cardiovasc Imaging*. 2017;10.
31. Grani C, Eichhorn C, Biere L, et al. Prognostic value of cardiac magnetic resonance tissue characterization in risk stratifying patients with suspected myocarditis. *J Am Coll Cardiol*. 2017;70:1964–1976.
32. Aquaro GD, Perfetti M, Camastra G, et al. Cardiac MR with late gadolinium enhancement in acute myocarditis with preserved systolic function: ITAMY study. *J Am Coll Cardiol*. 2017;70:1977–1987.
33. Aquaro GD, Ghebru Habtemicael Y, Camastra G, et al. Prognostic value of repeating cardiac magnetic resonance in patients with acute myocarditis. *J Am Coll Cardiol*. 2019;74:2439–2448.
34. Berg J, Kottwitz J, Baltensperger N, et al. Cardiac magnetic resonance imaging in myocarditis reveals persistent disease activity despite normalization of cardiac enzymes and inflammatory parameters at 3-month follow-up. *Circ Heart Fail*. 2017;10:e004262.
35. Kouranos V, Tzelepis GE, Rapti A, et al. Complementary role of CMR to conventional screening in the diagnosis and prognosis of cardiac sarcoidosis. *JACC Cardiovasc Imaging*. 2017;10:1437–1447.
36. Velangi PS, Chen KA, Kazmirczak F, et al. Right ventricular abnormalities on cardiovascular magnetic resonance imaging in patients with sarcoidosis. *JACC Cardiovasc Imaging*. 2020;13:1395–1405.
37. Coleman GC, Shaw PW, Balfour Jr PC, et al. Prognostic value of myocardial scarring on CMR in patients with cardiac sarcoidosis. *JACC Cardiovasc Imaging*. 2017;10:411–420.
38. Al-Khatib SM, Stevenson WG, Ackerman MJ, et al. 2017 AHA/ACC/HRS guideline for management of patients with ventricular arrhythmias and the prevention of sudden cardiac death: a report of the American College of Cardiology/American Heart Association Task Force on clinical practice guidelines and the heart rhythm society. *Circulation*. 2018;138:e272–e391.

39. Kotecha T, Martinez-Naharro A, Treibel TA, et al. Myocardial edema and prognosis in amyloidosis. *J Am Coll Cardiol*. 2018;71:2919–2931.
40. Pan JA, Kerwin MJ, Salerno M. Native T1 mapping, extracellular volume mapping, and late gadolinium enhancement in cardiac amyloidosis: a meta-analysis. *JACC Cardiovasc Imaging*. 2020;13:1299–1310.
41. Halliday BP, Cleland JGF, Goldberger JJ, Prasad SK. Personalizing risk stratification for sudden death in dilated cardiomyopathy: the past, present, and future. *Circulation*. 2017;136:215–231.
42. von Deuster C, Sammut E, Asner L, et al. Studying dynamic myofiber aggregate reorientation in dilated cardiomyopathy using in vivo magnetic resonance diffusion tensor imaging. *Circ Cardiovasc Imaging*. 2016;9:e005018.
43. Romano S, Judd RM, Kim RJ, et al. Feature-tracking global longitudinal strain predicts death in a multicenter population of patients with ischemic and nonischemic dilated cardiomyopathy incremental to ejection fraction and late gadolinium enhancement. *JACC Cardiovasc Imaging*. 2018;11:1419–1429.
44. Muthalaly RG, Kwong RY, John RM, et al. Left ventricular entropy is a novel predictor of arrhythmic events in patients with dilated cardiomyopathy receiving defibrillators for primary prevention. *JACC Cardiovasc Imaging*. 2019;12:1177–1184.
45. Alam MH, Auger D, McGill LA, et al. Comparison of 3 T and 1.5 T for T2* magnetic resonance of tissue iron. *J Cardiovasc Magn Reson*. 2016;18:40.
46. Scally C, Rudd A, Mezincescu A, et al. Persistent long-term structural, functional, and metabolic changes after stress-induced (Takotsubo) cardiomyopathy. *Circulation*. 2018;137:1039–1048.
47. Imran M, Wang L, McCrohon J, et al. Native T1 mapping in the diagnosis of cardiac allograft rejection: a prospective histologically validated study. *JACC Cardiovasc Imaging*. 2019;12:1618–1628.
48. Dolan RS, Rahsepar AA, Blaisdell J, et al. Multiparametric cardiac magnetic resonance imaging can detect acute cardiac allograft rejection after heart transplantation. *JACC Cardiovasc Imaging*. 2019;12:1632–1641.
49. Tello K, Dalmer A, Vanderpool R, et al. Cardiac magnetic resonance imaging-based right ventricular strain analysis for assessment of coupling and diastolic function in pulmonary hypertension. *JACC Cardiovasc Imaging*. 2019;12:2155–2164.
50. Galan-Arriola C, Lobo M, Vilchez-Tschischke JP, et al. Serial magnetic resonance imaging to identify early stages of anthracycline-induced cardiotoxicity. *J Am Coll Cardiol*. 2019;73:779–791.

Valvular Heart Disease

51. Woldendorp K, Bannon PG, Grieve SM. Evaluation of aortic stenosis using cardiovascular magnetic resonance: a systematic review & meta-analysis. *J Cardiovasc Magn Reson*. 2020;22:45.
52. Musa TA, Treibel TA, Vassiliou VS, et al. Myocardial scar and mortality in severe aortic stenosis. *Circulation*. 2018;138:1935–1947.
53. Everet RJ, Treibel TA, Fukui M, et al. Extracellular myocardial volume in patients with aortic stenosis. *J Am Coll Cardiol*. 2020;75:304–316.
54. Peterzan MA, Clarke WT, Lygate CA, et al. Cardiac energetics in patients with aortic stenosis and preserved versus reduced ejection fraction. *Circulation*. 2020;141:1971–1985.
55. Cavalcante JL, Rijal S, Abdelkarim I, et al. Cardiac amyloidosis is prevalent in older patients with aortic stenosis and carries worse prognosis. *J Cardiovasc Magn Reson*. 2017;19:98.
56. Kammerlander AA, Wiesinger M, Duca F, et al. Diagnostic and prognostic utility of cardiac magnetic resonance imaging in aortic regurgitation. *JACC Cardiovasc Imaging*. 2019;12:1474–1483.
57. Uretsky S, Argulian E, Narula J, Wolff SD. Use of cardiac magnetic resonance imaging in assessing mitral regurgitation: current evidence. *J Am Coll Cardiol*. 2018;71:547–563.
58. Penicka M, Vecera J, Mirica DC, et al. Prognostic implications of magnetic resonance-derived quantification in asymptomatic patients with organic mitral regurgitation: comparison with Doppler echocardiography-derived integrative approach. *Circulation*. 2018;137:1349–1360.
59. Kitkungvan D, Nabi F, Kim RJ, et al. Myocardial fibrosis in patients with primary mitral regurgitation with and without prolapse. *J Am Coll Cardiol*. 2018;72:823–834.
60. Cavalcante JL, Kusunose K, Obuchowski NA, et al. Prognostic impact of ischemic mitral regurgitation severity and myocardial infarct quantification by cardiovascular magnetic resonance. *JACC Cardiovasc Imaging*. 2020;13:1489–1501.
61. Zhan Y, Senapati A, Vejpongpa P, et al. Comparison of echocardiographic assessment of tricuspid regurgitation against cardiovascular magnetic resonance. *JACC Cardiovasc Imaging*. 2020;13:1461–1471.

Pericardial Disease; Cardiac Electrophysiology; Novel Techniques

62. Kumar A, Sato K, Yzeiraj E, et al. Quantitative pericardial delayed hyperenhancement informs clinical course in recurrent pericarditis. *JACC Cardiovasc Imaging*. 2017;10:1337–1346.
63. Acosta J, Fernandez-Armenta J, Borras R, et al. Scar characterization to predict life-threatening arrhythmic events and sudden cardiac death in patients with cardiac resynchronization therapy: the GAUDI-CRT study. *JACC Cardiovasc Imaging*. 2018;11:561–572.
64. Hirai K, Kido T, Kido T, et al. Feasibility of contrast-enhanced coronary artery magnetic resonance angiography using compressed sensing. *J Cardiovasc Magn Reson*. 2020;22:15.
65. Schukro C, Puchner SB. Safety and efficiency of low-field magnetic resonance imaging in patients with cardiac rhythm management devices. *Eur J Radiol*. 2019;118:96–100.
66. Simonetti OP, Ahmad R. Low-field cardiac magnetic resonance imaging: a compelling case for cardiac magnetic resonance's future. *Circ Cardiovasc Imaging*. 2017;10:e005446.